The intra-mitochondrial contact site formed by Cqd1 and the Por1-Om14 complex modulates architecture and morphology of mitochondria

Siavash Khosravi[1], Xenia Chelius[2], Ann-Katrin Unger[2], Timo Sachsenheimer[3], Christian Lüchtenborg[3], Rico Schieweck[1], Britta Brügger[3], Benedikt Westermann[2], Till Klecker[2], Walter Neupert[1,‡] and Max E. Harner[1]

[1] Department of Cell Biology, Biomedical Center, Medical Faculty, Ludwig-Maximilians University Munich, 82152 Planegg/Martinsried, Germany

[2] Institute of Cell Biology, University of Bayreuth, 95440 Bayreuth, Germany

[3] Heidelberg University Biochemistry Center (BZH), 69120 Heidelberg, Germany

[‡] Deceased

Corresponding author: Max E. Harner

Mailing address: Großhaderner Str. 9, 82152 Planegg/Martinsried, Germany

Fax: +49 89 2180 75882

Phone: +49 89 2180 71885

e-mail address: max.harner@bmc.med.lmu.de

Abstract

Mitochondria are essential organelles of eukaryotic cells that are characterized by their unique and complex membrane system. They are confined from the cytosol by an envelope consisting of two membranes. Signals, metabolites, proteins and lipids have to be transferred across these membranes via proteinaceous contact sites to keep mitochondria functional. In the present study we identified a novel mitochondrial contact site that is formed by Cqd1 in the inner membrane and the outer membrane complex Por1-Om14. Cqd1 is a member of the highly conserved UbiB protein kinase-like family (also called aarF domain containing kinases). It was recently shown that Cqd1 in cooperation with Cqd2 controls the cellular distribution of coenzyme Q by a yet unknown mechanism. Our data suggest that Cqd1 besides its known function in coenzyme Q homeostasis is involved in the homeostasis of phospholipids, the organization of the mitochondrial inner membrane and the interaction of mitochondria with the endoplasmic reticulum.

Introduction

Mitochondria are essential organelles in eukaryotic cells and are characterized by an envelope consisting of two membranes. In addition to their important role in the cellular energy metabolism, mitochondria perform a multitude of other functions, including the synthesis of proteins, iron-sulfur clusters and lipids. Specialized structures in the mitochondrial membranes, so-called contact sites, have to be present to enable mitochondria to perform all these functions. The term contact site often refers to inter-organellar contacts, for instance between mitochondria and the endoplasmic reticulum (ER) (Kornmann et al., 2009; Murley et al., 2015), mitochondria and vacuoles, the yeast equivalent of mammalian lysosomes (Gonzalez Montoro et al., 2018; John Peter et al., 2017), or mitochondria and lipid droplets (Pu et al., 2011). In addition, intra-mitochondrial contact sites between the mitochondrial inner and outer membrane can be observed (Tamura et al., 2019). Importantly, both kinds of contacts are crucial for mitochondrial functions (Khosravi and Harner, 2020; Klecker et al., 2014; Kornmann, 2020; Phillips and Voeltz, 2016; Renne and Hariri, 2021; Vyssokikh and Brdiczka, 2003).

Most contacts between the mitochondrial inner and outer membrane depend on the mitochondrial contact site and cristae organizing system (MICOS), a multi-subunit protein complex in the mitochondrial inner membrane (Harner et al., 2011; Hoppins et al., 2011; von der Malsburg et al., 2011). This highly conserved complex interacts with at least six different proteins or complexes of the outer membrane: the Fzo1-Ugo1 complex (Harner et al., 2011), the Miro GTPases (Modi et al., 2019), Om45 (Hoppins et al., 2011), Por1 (Hoppins et al., 2011), the TOB (SAM) complex (Bohnert et al., 2012; Darshi et al., 2011; Harner et al., 2011; Korner et al., 2012; Xie et al., 2007; Zerbes et al., 2012) and the TOM complex (Bohnert et al., 2012; von der Malsburg et al., 2011; Zerbes et al., 2012).

In addition, several other intra-mitochondrial contact sites exist that do not depend on MICOS. Some of these have been known for decades, like the TIM23-TOM super complex (Chacinska et al., 2003; Dekker et al., 1997; Schleyer and Neupert, 1985; Schwaiger et al., 1987), the mitochondrial permeability transition pore consisting of the ADP-ATP carrier (ANT), the mitochondrial creatine kinase and VDAC (mammalian porin) (Beutner et al., 1996; Vyssokikh and Brdiczka, 2003) or the mitochondrial fusion machineries (Fritz et al., 2001; Sesaki et al., 2003; Wong et al., 2003). Others were identified just recently, for instance the contact site formed by Por1 (yeast porin) and Mdm31 that was suggested to be important for the biosynthesis of cardiolipin (Miyata et al., 2018). Apparently, the functions of these intra-mitochondrial contacts are quite diverse, varying from protein import to signal transduction, lipid transport and the formation of mitochondrial architecture and morphology.

Members of the poorly characterized UbiB protein kinase-like family (aarF domain containing kinases) were recently implicated in mitochondrial membrane homeostasis (Awad et al., 2020; Johnson et al., 2005; Kemmerer et al., 2021; Mollet et al., 2008; Odendall et al., 2019; Reidenbach et al., 2018; Stefely

et al., 2015). UbiB family members are defined by the presence of a protein kinase-like domain (PKL) of unknown function. *Saccharomyces cerevisiae* has three family members which all reside in mitochondria: Coq8 (Abc1), Cqd1 (Mco76) and Cqd2 (Mcp2) (Do et al., 2001; Morgenstern et al., 2017; Tan et al., 2013). The bacterial proteins UbiB (*Escherichia coli*) and AarF (*Providencia stuartii*) are essential for the synthesis of coenzyme Q (ubiquinone) (Macinga et al., 1998; Poon et al., 2000). Likewise, Coq8 and its mammalian homolog ADCK3 are also part of the coenzyme Q biosynthesis pathway (Do et al., 2001; Johnson et al., 2005; Mollet et al., 2008; Reidenbach et al., 2018; Stefely et al., 2015). While our work was in progress an elegant study linked Cqd1 and Cqd2 also to coenzyme Q homeostasis. Deletion of *CQD1* results in excess export of coenzyme Q to extra-mitochondrial membranes, whereas deletion of *CQD2* leads to an accumulation of excess coenzyme Q in mitochondria. Thus, Cqd1 and Cqd2 apparently perform antagonistic roles in the distribution of coenzyme Q between mitochondria and other organelles (Kemmerer et al., 2021). However, the molecular mechanism of Cqd1 and Cqd2 function in cellular coenzyme Q distribution remained unknown.

In the present study, we set out to functionally analyze the conserved and poorly characterized mitochondrial protein encoded by the ORF *YPL109C*, which is now named Cqd1. We identified a MICOS-independent contact site formed by Cqd1 in the mitochondrial inner membrane and Por1 and Om14 in the outer membrane. Furthermore, we show that Cqd1 participates in the formation of mitochondrial architecture and morphology. Our results support a model in which the activity of Cqd1 contributes to the regulation of the distribution of mitochondrial lipids and membrane architecture at a novel mitochondrial membrane contact site.

Results

Cqd1 is a mitochondrial inner membrane protein facing the intermembrane space

We first asked where Cqd1 is precisely located within mitochondria. *In silico* analysis using MitoProt II (Claros and Vincens, 1996) revealed that Cqd1 contains a potential N-terminal mitochondrial targeting sequence (MTS; amino acids 1-15) (Fig. 1A). In addition, two hydrophobic stretches can be identified in the Cqd1 sequence, of which the first one (amino acids 125-142) might be a *bona fide* transmembrane segment (Fig. 1A). We used an epitope-tagged construct (Cqd1-3xHA) to analyze the topology of Cqd1. Proteinase K (PK) accessibility and alkaline extraction assays using isolated mitochondria showed that it is behaving like Tim50 which is anchored in the inner membrane with an α-helical transmembrane domain (Fig. 1B and C). PK did not degrade Cqd1-3xHA in intact mitochondria, but the signal was largely gone when PK was added to hypotonically swollen mitochondria with a disrupted outer membrane. No shorter fragment appeared upon addition of PK

106 to swollen mitochondria indicating that the C-terminal tag was degraded (Fig. 1B). Furthermore, Cqd1-
107 3xHA remained in the pellet fraction upon alkaline extraction like the membrane proteins Tom70 and
108 Tim50 (Fig. 1C). It should be noted that in Western blot analyses Cqd1-3xHA showed an apparent size
109 of 66 kDa, instead of its calculated molecular weight of 76 kDa (untagged Cqd1 full length) or 74 kDa
110 (untagged Cqd1 minus MTS) (Fig. 1B and C). We conclude that Cqd1 is present in the mitochondrial
111 inner membrane with its major C-terminal part facing the intermembrane space.

112
113
114
115
116
117
118
119
120
121
122
123
124
125
126
127

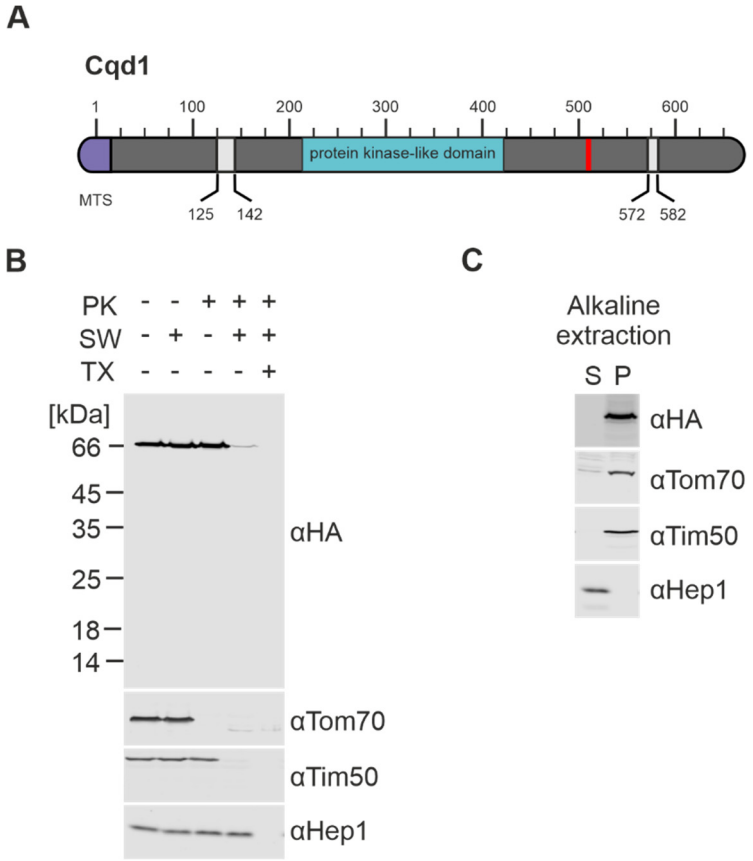

Figure 1. **Cqd1 is a mitochondrial inner membrane protein exposing its C terminus to the intermembrane space.** **(A)** Schematic representation of Cqd1. Violet, mitochondrial targeting sequence (MTS; amino acids 1-15); light grey, hydrophobic regions (amino acids 125-142 and 572-582); red, conserved GxxxG dimerization motif (amino acids 504-508); turquoise, conserved protein kinase-like domain (amino acids 213-421). **(B)** Cqd1 exposes its C terminus to the intermembrane space. Mitochondria isolated from a Cqd1-3xHA expressing strain were treated with isotonic buffer, subjected to swelling by incubation in hypotonic buffer to disrupt the outer membrane (SW), or lysed using a Triton X-100 containing buffer (TX). Proteinase K (PK) was added as indicated. Samples were analyzed by SDS-PAGE and immunoblotting. Tom70, marker for the outer membrane; Tim50, marker for the inner membrane; Hep1, soluble marker protein for the matrix. **(C)** Cqd1 is an integral membrane protein. Isolated mitochondria were subjected to alkaline extraction to separate soluble and membrane proteins. Soluble proteins present in the supernatant (S) and membrane proteins in the pellet (P) were analyzed by SDS-PAGE and immunoblotting.

128

129 **The *CQD1* gene negatively interacts with *UPS1* and *CRD1***

130 Several high-throughput screens showed that cells lacking Cqd1 are able to grow on non-fermentable
131 carbon sources (Qian et al., 2012; Stenger et al., 2020). Also, Kemmerer et al. (2021) observed growth

132 of Δ*cqd1* cells under respiratory conditions in liquid media, albeit growth was reduced when coenzyme
133 Q precursors were depleted. We generated a deletion mutant lacking Cqd1 and analyzed its growth
134 phenotype under several conditions on agar plates. We observed that the Δ*cqd1* mutant grows like
135 wild type on fermentable and non-fermentable carbon sources at normal and elevated temperatures
136 (Fig. 2A) confirming that Cqd1 is not essential for respiratory growth.
137 Mitochondria are intensively involved in the cellular phospholipid metabolism by generating
138 cardiolipin and phosphatidylethanolamine. Interestingly, two independent high-throughput studies
139 revealed a genetic interaction of *CQD1* with *UPS1* (Costanzo et al., 2016; Hoppins et al., 2011). Ups1 is
140 responsible for transport of phosphatidic acid across the intermembrane space (Fig. 2B) (Connerth et
141 al., 2012; Tamura et al., 2012). Thus, we generated double deletion mutants lacking *CQD1* and genes
142 encoding proteins involved in mitochondrial phospholipid metabolism, including *CLD1*, *CRD1*, *GEP4*,
143 *MDM35*, *PGS1*, *PSD1*, *TAM41*, *TAZ1*, *UPS1* and *UPS2* (Fig. 2B). Growth analysis revealed a strong defect
144 of the double deletion mutant Δ*cqd1* Δ*ups1* specifically on synthetic medium. A weaker yet
145 reproducible growth defect at 37°C could be detected for the double deletion mutant Δ*cqd1* Δ*crd1*. All
146 other double deletion mutants did not show an enhanced growth phenotype. The growth defect of
147 the single deletion mutants Δ*tam41* and Δ*pgs1* was so strong that we cannot judge whether the
148 additional deletion of *CQD1* further reduces cell growth (Fig. 2C).
149 Cqd1 is a member of the highly conserved UbiB family (Kemmerer et al., 2021; Stefely et al., 2015) and
150 thus shows a predicted protein kinase-like domain (amino acids 213-421, Saccharomyces Genome
151 Database, SGD (Cherry et al., 2012) (Fig. 1A). Therefore, we asked whether the protein kinase-like
152 domain of Cqd1 is important for its function. We generated mutants in conserved amino acid residues
153 within this domain (K275A, D288A and E330A) to inhibit ATP binding similar to what was done before
154 in studies on Cqd2 and Coq8 (Odendall et al., 2019; Reidenbach et al., 2018; Stefely et al., 2015). Of
155 note, introduction of the point mutations K275A or D288A led to strongly reduced steady state levels
156 of Cqd1 indicating reduced expression or stability of the protein (Fig. 2D). Thus, we did not further
157 analyze these alleles. In contrast, the introduction of the point mutation E330A did not affect the
158 steady state level of Cqd1 (Fig. 2D). While expression of wild type Cqd1 largely restored the growth of
159 the double deletion mutant Δ*cqd1* Δ*ups1*, the *cqd1(E330A)* allele did not, indicating that ATP binding
160 of Cqd1 is important for its function (Fig. 2E). These results are in accordance with observations
161 recently made by Kemmerer et al. (2021) who reported that alleles carrying mutations of conserved
162 residues of the kinase-like domain were unable to rescue Δ*cqd1* growth defects.
163 In sum, we could manually confirm the negative genetic interaction of *CQD1* and *UPS1* and identified
164 *CRD1* as a novel negative interactor of *CQD1*. Interestingly, both genetic interactors are involved in
165 biosynthesis of the phospholipid cardiolipin. Furthermore, Cqd1 activity depends on an intact protein
166 kinase-like domain.

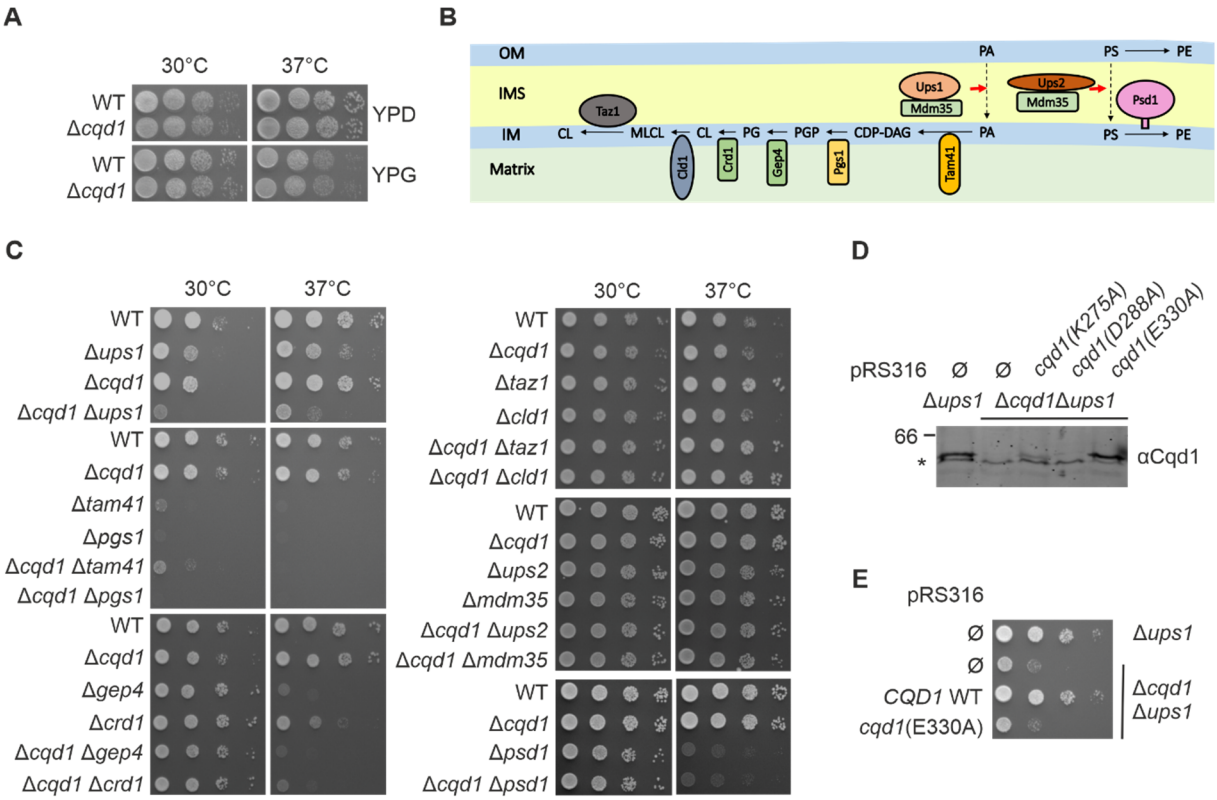

Figure 2. *CQD1* is a negative genetic interactor of *UPS1* and *CRD1*.

(A) Deletion of *CQD1* does not result in a growth defect. Cells of wild type and a Δ*cqd1* deletion strain were grown to logarithmic growth phase in rich medium containing glucose as carbon source (YPD). Cell growth was analyzed by drop dilution assay on plates containing rich medium supplemented with either glucose (YPD) or glycerol (YPG) at 30°C or 37°C. **(B)** Schematic illustration of the mitochondrial phospholipid metabolism. IM, inner membrane; IMS, intermembrane space; OM, outer membrane; CDP-DAG, cytidine diphosphate diacylglycerol; CL, cardiolipin; MLCL, monolysocardiolipin; PA, phosphatidic acid; PE, phosphatidylethanolamine; PG, phosphatidylglycerol; PGP, phosphatidylglycerol phosphate; PS, phosphatidylserine. **(C)** Deletion of *CQD1* from cells lacking Ups1 or Crd1 results in a synthetic growth defect. Cells were treated as in (A) with the difference that they were shifted to synthetic medium containing glucose (SCD) 30 h before growth analysis on SCD plates. **(D)** The conserved amino acids K275 and D288 in the predicted protein kinase-like domain are important for the stability of Cqd1. Cells bearing either the empty plasmid (Ø) or plasmids carrying the respective *cqd1* alleles were grown in SCD. Crude mitochondria were isolated and the Cqd1 levels were analyzed by immunoblotting using an anti-Cqd1 antibody. The asterisk indicates a cross reaction of the anti-Cqd1 antibody. **(E)** Glutamic acid 330 is essential for the function of Cqd1. Cells bearing either the empty plasmid or a plasmid carrying *CQD1* wild type (WT) or *cqd1(E330A)* alleles were treated as in (C).

Cqd1 contributes to mitochondrial lipid homeostasis

Next, we analyzed the phospholipid composition of mitochondria isolated from wild type yeast, the Δ*ups1* or Δ*cqd1* single deletion strains and the Δ*cqd1* Δ*ups1* double deletion mutant by mass spectrometry. Consistent with previous results (Connerth et al., 2012), deletion of *UPS1* results in a severe reduction of cardiolipin and monolysocardiolipin (Fig. 3, Suppl. Table 1). Also, we observed a significant reduction of phosphatidic acid in Δ*ups1*, which might depend on growth conditions (Eiyama

189 et al., 2021). Interestingly, the lipidomics analysis of mitochondria obtained from Δ*cqd1* revealed a
190 significant reduction of phosphatidic acid while other phospholipids remained unchanged (Fig. 3,
191 Suppl. Table 1). The double deletion mutant Δ*cqd1* Δ*ups1* did not show a synthetic phenotype. We
192 suggest that Cqd1 is involved not only in maintenance of mitochondrial coenzyme Q levels (Kemmerer
193 et al., 2021), but also modulates the levels of phosphatidic acid (Fig. 3, Suppl. Table 1) and possibly
194 other lipids.

195
196
197
198
199

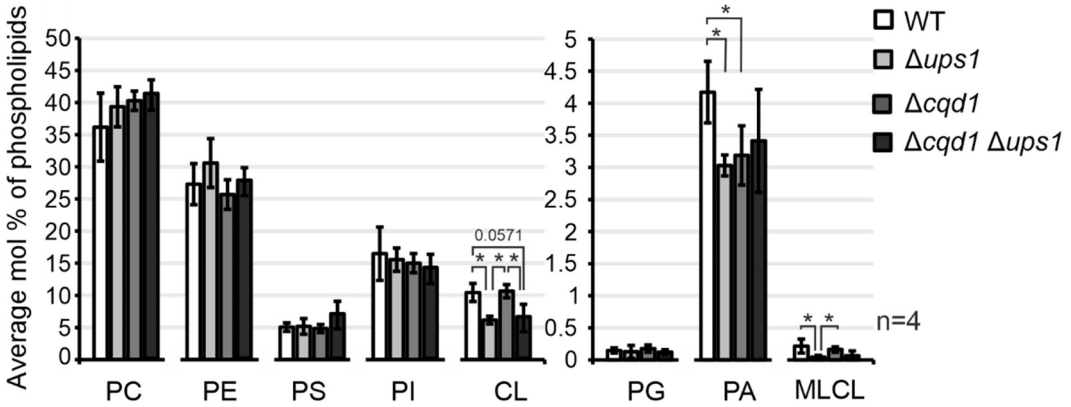

Figure 3. Cqd1 is involved in mitochondrial phospholipid homeostasis.

Strains were grown in synthetic medium containing glycerol (SCG) and mitochondria were purified by sucrose gradient centrifugation. Phospholipids were extracted and analyzed by mass spectrometry. The level of each phospholipid species (% of total phospholipids) is shown as a mean of four independently performed experiments with standard deviation bars. Asterisks represent p-values obtained by Mann Whitney test (*p≤0.05). CL, cardiolipin; MLCL, monolysocardiolipin; PA, phosphatidic acid; PC, phosphatidylcholine; PE, phosphatidylethanolamine; PG, phosphatidylglycerol; PI, phosphatidylinositol; PS, phosphatidylserine.

200

201 **Mitochondrial biogenesis and dynamics are impaired in the Δ*cqd1* Δ*ups1* double mutant**

202 The drastic growth phenotype of the Δ*cqd1* Δ*ups1* double mutant (Fig. 2C) suggests that this strain
203 struggles with severe problems in essential mitochondrial functions which might be caused by a lack
204 of mitochondrial proteins or complexes involved in mitochondrial dynamics, architecture, protein
205 import or respiration. Therefore, we analyzed the steady state levels of various proteins involved in
206 these processes, including Fzo1, Ugo1, Mic27, Mic60, Tim23, Tim50, Rip1 and Cor2. Also, we tested
207 assembly of the TOM complex and the respiratory chain super complexes by native gel electrophoresis.
208 However, a comparison of the Δ*cqd1* Δ*ups1* double mutant with wild type and the single deletion
209 mutants revealed no significant defects (Fig. 4A and B).

210 Previous studies showed that deletion of *UPS1* compromises two processes that both depend on the
211 mitochondrial membrane potential. First, the import of the mitochondrial matrix-localized chaperone
212 Mdj1 is impaired resulting in the accumulation of unprocessed precursor (Tamura et al., 2009). And
213 second, processing of Mgm1, a large inner membrane-associated GTPase required for mitochondrial
214 fusion, is reduced resulting in the accumulation of the long isoform, l-Mgm1 (Sesaki et al., 2006). We

found that both defects are exacerbated in the Δ*cqd1* Δ*ups1* double mutant. We observed a strong accumulation of Mdj1 precursor protein and an almost complete inhibition of Mgm1 processing (Fig. 4C and D). Previous studies showed that a balanced ratio of processed s-Mgm1 to unprocessed l-Mgm1 is necessary for mitochondrial fusion (DeVay et al., 2009; Zick et al., 2009). Accordingly, we observed an almost complete fragmentation of the mitochondrial network in the double deletion mutant Δ*cqd1* Δ*ups1*, indicating impairment of mitochondrial fusion (Fig. 4E). Thus, the relative mild phenotypes of the Δ*ups1* single deletion mutant regarding cell growth, generation of membrane potential and morphology of mitochondria (Sesaki et al., 2006; Tamura et al., 2009) are enhanced by additional deletion of the *CQD1* gene.

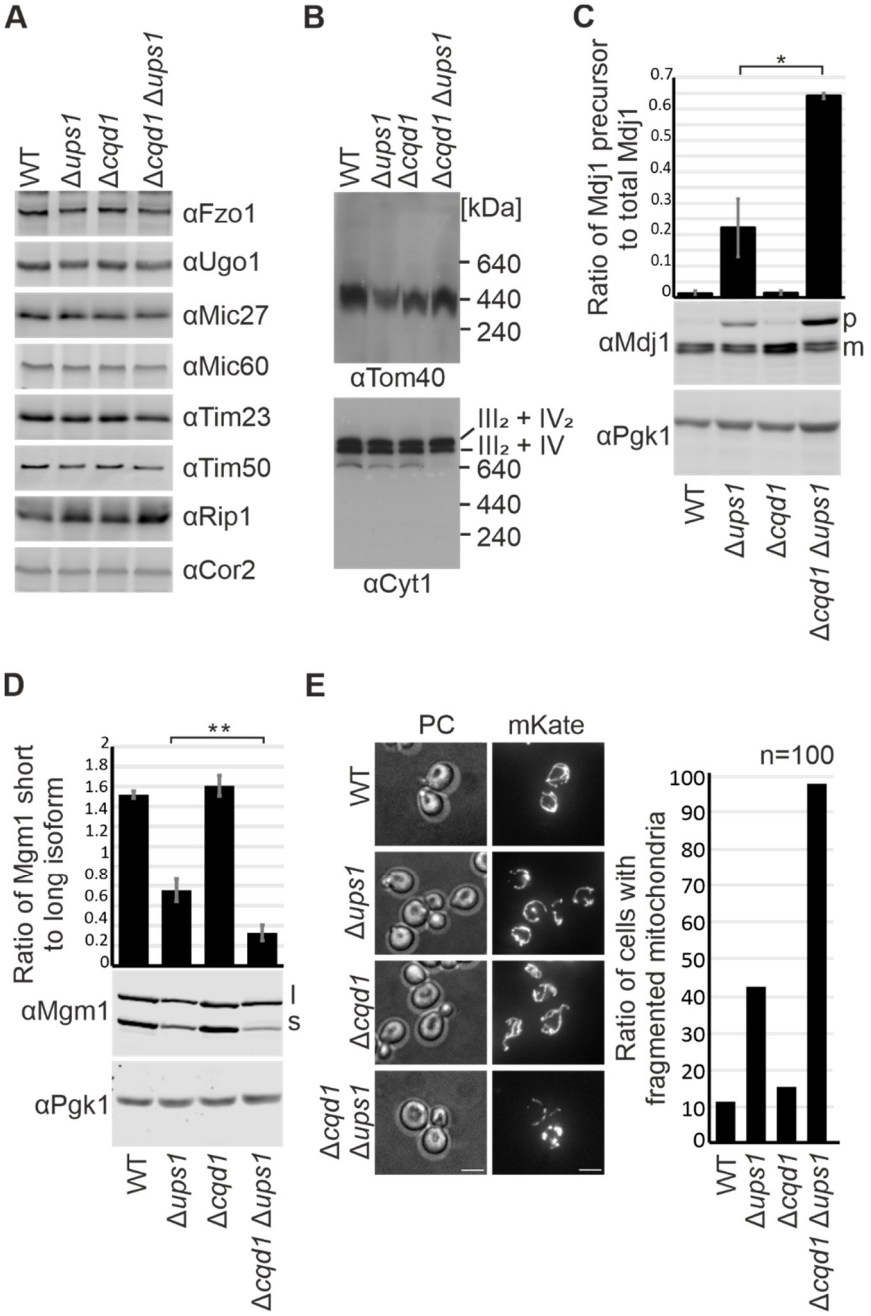

Figure 4. Simultaneous deletion of *CQD1* and *UPS1* compromises mitochondrial function.

(A) Analysis of steady state levels of mitochondrial proteins in wild type cells and cells lacking Ups1, Cqd1, or both. Cells were grown in synthetic medium, and whole cell extracts were analyzed by immunoblotting. **(B)** Formation of mitochondrial protein complexes. Strains were grown in SCG. Isolated mitochondria were lysed in digitonin-containing buffer (3% w/v) and cleared lysates were subjected to BN-PAGE. The assembly of the TOM complex and respiratory chain super complexes were analyzed by immunoblotting using antibodies against Tom40 or Cyt1. **(C)** Deletion of *CQD1* in cells lacking Ups1 exacerbates accumulation of the precursor of Mdj1. Cells were grown in SCD, whole cell lysates were prepared and analyzed by immunoblotting with specific antibodies. Pgk1 served as a loading control. p, precursor of Mdj1; m, mature form of Mdj1. The quantification was obtained from three independent experiments and shows means of the ratio of the Mdj1 precursor to the total amount of Mdj1. Error bars indicate standard deviation. Asterisk represents p-value obtained by unpaired Student's t test (*p≤0.05). **(D)** Simultaneous deletion of *CQD1* and *UPS1* leads to strongly reduced processing of Mgm1. Whole cell lysates from cells grown in SCD were analyzed by immunoblotting. l, long isoform of Mgm1; s, short isoform of Mgm1. The quantification was obtained from three independent experiments and shows means of the ratio of the short form to the long form of Mgm1. Asterisks represent p-values obtained by unpaired Student's t test (**p≤0.01). **(E)** Mitochondria in cells lacking Ups1 and Cqd1 are highly fragmented. Mitochondria were labeled by expression of mKate targeted to mitochondria. Cells were grown in YPD and shifted to SCD, harvested in their logarithmic growth phase and immobilized on slides covered with concanavalin A. Scale bars, 4 µm. PC, phase contrast. For quantification 100 cells were counted for each strain.

Cqd1 and Cqd2 have antagonistic roles in mitochondrial biogenesis

Previous studies indicated opposing functions of Cqd1 and Cqd2 (Kemmerer et al., 2021). Therefore, we generated all possible single, double and triple deletion mutants to analyze the interaction network of *CQD1*, *CQD2* and *UPS1*. Strikingly, growth analysis of the triple deletion mutant Δ*cqd1* Δ*ups1* Δ*cqd2* revealed that deletion of *CQD2* in the Δ*cqd1* Δ*ups1* background completely rescued the growth phenotype (Fig. 5A). At the same time, the accumulation of Mdj1 precursor protein and the impaired Mgm1 processing were largely rescued (Fig. 5B and C). This suggests that the equilibrium of the putative kinases Cqd1 and Cqd2 is particularly important when mitochondrial membrane lipid composition is disturbed through deletion of *UPS1*.

Cqd1 is part of a MICOS-independent contact site

Our results described above and the observations reported by Kemmerer et al. (2021) suggest that Cqd1 is involved in mitochondrial lipid homeostasis. We reasoned that a membrane contact site would be ideally suited for such a function. To test whether Cqd1 is a contact site protein, we used an established method to fractionate mitochondria, which is based on sonication, dounce homogenization and subsequent density gradient centrifugation of mitochondrial particles (Harner et al., 2011). Strikingly, Western blot analysis of mitochondrial fractions revealed that the distribution of Cqd1 is clearly distinguishable from both the outer membrane marker Tom40 and the inner membrane

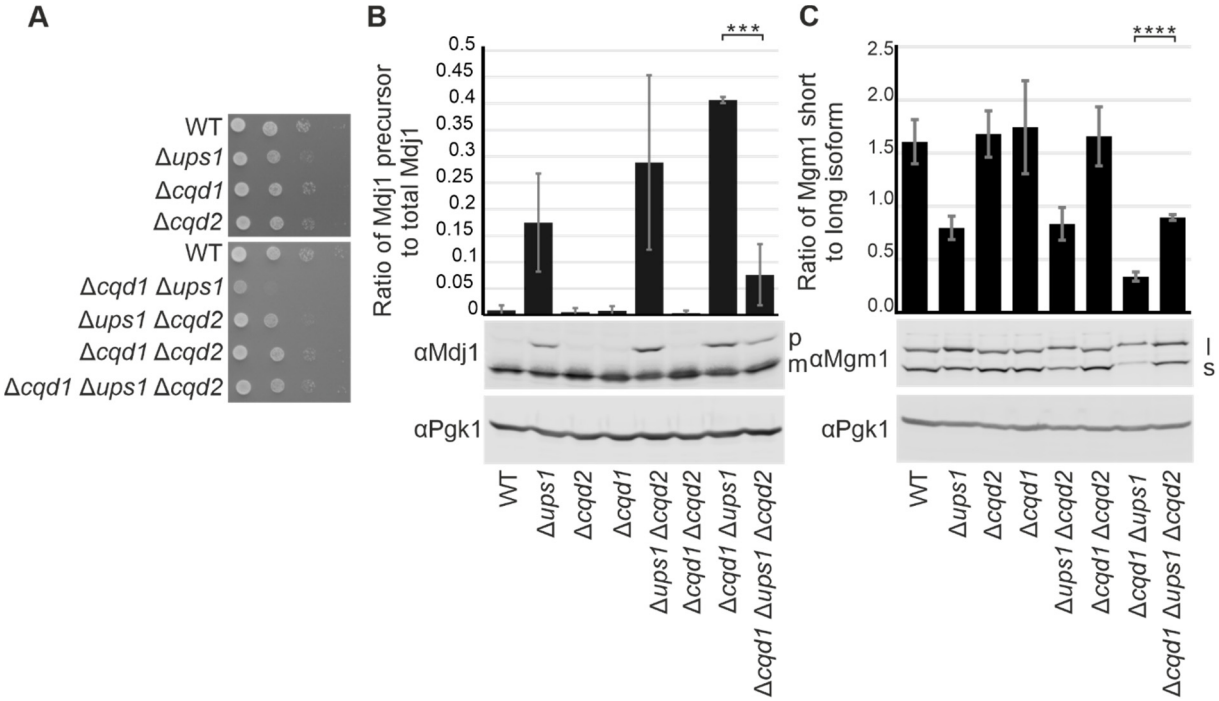

Figure 5. Deletion of *CQD2* restores the phenotypes of a Δ*cqd1* Δ*ups1* double deletion.

(A) Deletion of *CQD2* in the Δ*cqd1* Δ*ups1* background rescues the growth phenotype. Strains were grown to logarithmic phase and growth was analyzed by drop dilution assay on SCD plates at 30°C. **(B+C)** Mdj1 import and Mgm1 processing is restored in the Δ*cqd1* Δ*ups1* Δ*cqd2* triple mutant. Cells were grown in SCD, whole cell lysates were prepared and analyzed by immunoblotting. Pgk1 served as a loading control. **(B)** p, precursor of Mdj1; m, mature form of Mdj1. The quantification was obtained from three independent experiments and shows means of the ratio of the Mdj1 precursor to the total amount of Mdj1. **(C)** l, long isoform of Mgm1; s, short isoform of Mgm1. The quantification was obtained from three independent experiments and shows means of the ratio of the short form to the long form of Mgm1. Error bars indicate standard deviation. Asterisks represent p-values obtained by unpaired Student's t test (***p≤0.001; ****p≤0.0001).

marker Tim17. Cqd1 was enriched in fractions of intermediate density very similar to the MICOS subunit Mic27 (Fig. 6A and Suppl. Fig. 1). In order to analyze whether Cqd1 is a novel MICOS subunit we performed immunoprecipitation of Cqd1 and different MICOS subunits. Neither the isolation of Cqd1 resulted in co-isolation of the MICOS subunits Mic10 or Mic60 nor vice versa (Fig. 6B and C). Native gel electrophoresis revealed that Cqd1 is present in a high molecular weight complex of ca. 400 kDa. A small, yet reproducible fraction was detectable at approximately 650 kDa (Fig. 6D), a size that is clearly different from the 1.5 MDa large MICOS complex (Alkhaja et al., 2012; Harner et al., 2011; von der Malsburg et al., 2011). These results suggest that Cqd1 is part of a novel contact site rather than a new MICOS subunit.

To screen for possible interaction partners of Cqd1 we first tested whether it might interact homotypically because it contains a highly conserved GxxxG dimerization motif (amino acids 504-508, Fig. 1A). To this end a yeast strain was generated expressing simultaneously a 3xHA-tagged and a

3xMyc-tagged version of Cqd1. Immunoprecipitation of Cqd1-3xHA led to efficient co-isolation of Cqd1-3xMyc, revealing homotypic interactions of Cqd1 (Fig. 6E).

While the homotypic Cqd1 interaction could explain the formation of the high molecular weight complex (Fig. 6D), it does not explain the presence of Cqd1 in contact site fractions (Fig. 6A). Therefore, chemical crosslinking was used to get an indication of further interaction partners. While incubation with Di(N-succinimidyl) glutarate (DSG) did not reveal any crosslink partners, treatment with m-maleimidobenzoyl-N-hydoxysuccinimide ester (MBS) produced two prominent crosslinks (Fig. 6F).

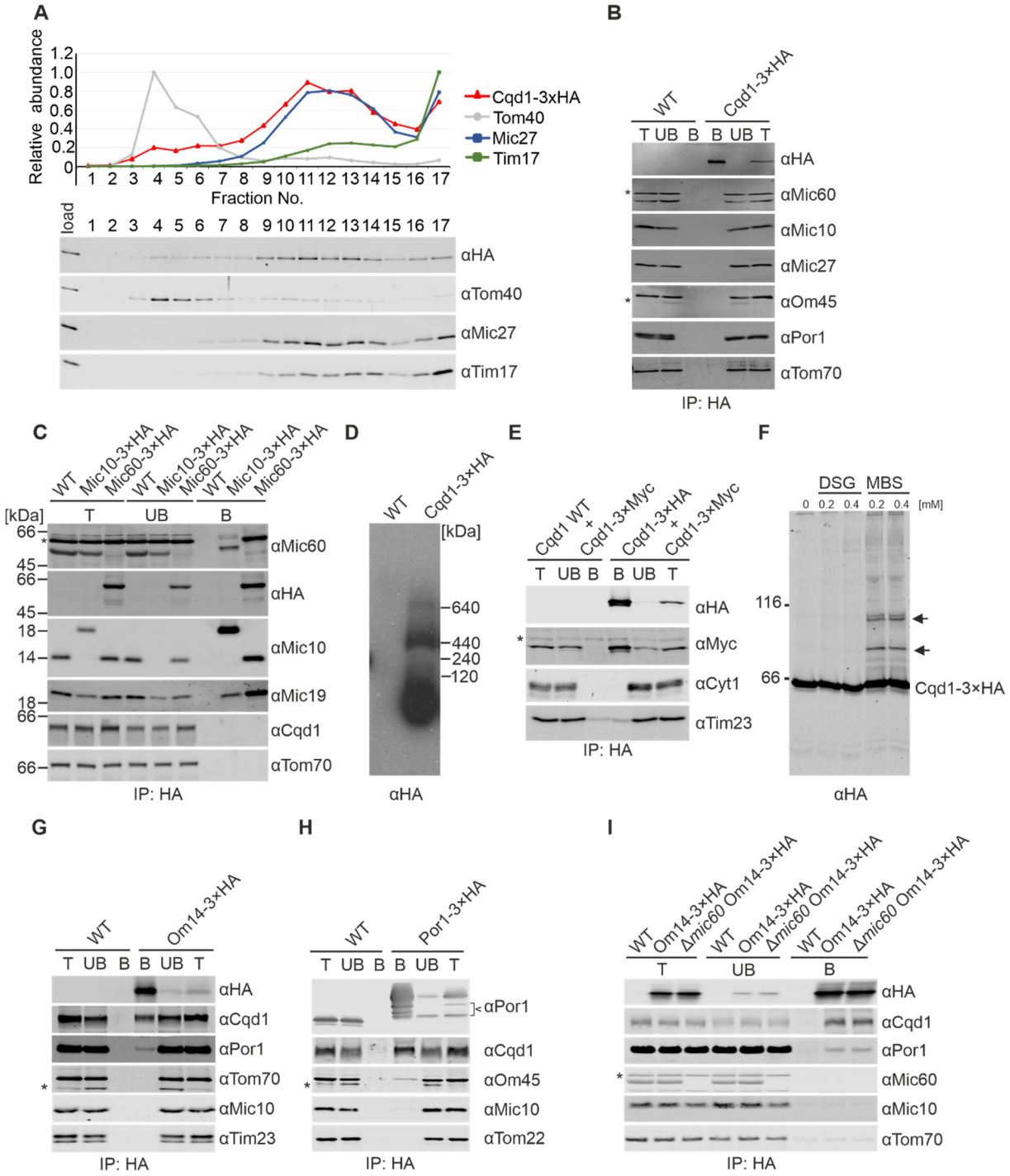

Figure 6. Cqd1 forms a novel contact site with Om14 and Por1.

(A) Cqd1 is enriched in contact site fractions. Mitochondria of a Cqd1-3xHA expressing strain were isolated, subjected to osmotic shrinking, sonication, and sucrose density gradient centrifugation. The gradient was fractionated, proteins were subjected to TCA precipitation and analyzed by immunoblotting. (Top) The graph shows mean values of three independent experiments for the distribution of Cqd1-3xHA and the marker proteins for the outer membrane (Tom40), the inner membrane (Tim17) or contact sites (Mic27). Error bars indicating standard deviations are shown in Suppl. Fig. 1. (Bottom) Immunodecorations of one representative experiment. **(B)** Mic10 and Mic60 do not co-precipitate with Cqd1. Mitochondria of wild type and a yeast strain expressing Cqd1-3xHA were isolated and lysed in digitonin containing buffer (1% w/v). Lysates were subjected to immunoprecipitation using anti-HA affinity agarose. T, total lysate (5%); UB, unbound protein (5%); B, bound protein (100%) were analyzed by immunoblotting. Asterisks indicate cross reactions of the antibodies against Mic60 or Om45. **(C)** Cqd1 does not co-precipitate with Mic10 or Mic60. Mitochondria of wild type or yeast strains expressing Mic10-3xHA or Mic60-3xHA were analyzed as in (B). T, total lysate (2.5%); UB, unbound protein (2.5%); B, bound protein (100%). The asterisk indicates a cross reaction of the anti-Mic60 antibody. Since the cross reaction of the Mic60 antibody shows the same size as Mic60-3xHA, a decoration of this membrane fragment with an anti-HA antibody is presented additionally. **(D)** Cqd1 forms high molecular weight complexes. Mitochondria isolated from wild type and a yeast strain expressing Cqd1-3xHA were solubilized in digitonin (3% w/v). Cleared lysates were subjected to BN-PAGE. Cqd1-3xHA containing complexes were detected by immunoblotting with an anti-HA antibody. **(E)** Cqd1 interacts homotypically. Mitochondria of yeast strains expressing Cqd1-3xMyc in the presence of untagged or 3xHA tagged Cqd1 were treated as described in (B). T, total lysate (5%); UB, unbound protein (5%); B, bound protein (100%). The asterisk indicates a cross reaction of the anti-Myc antibody. **(F)** Cqd1 interacts with other proteins than itself. Isolated mitochondria of a Cqd1-3xHA expressing strain were exposed to DMSO or the chemical crosslinkers DSG and MBS at the indicated concentrations. Samples were analyzed by immunoblotting with an anti-HA antibody. Arrows indicate Cqd1-containing crosslinks. **(G)** Cqd1 interacts with Om14. Mitochondria of wild type and a yeast strain expressing Om14-3xHA were analyzed as in (B). T, total lysate (1%); UB, unbound protein (1%); B, bound protein (100%). The asterisk indicates a cross reaction of the anti-Tom70 antibody. **(H)** Cqd1 interacts with Por1. Mitochondria of wild type or a yeast strain expressing Por1-3xHA were analyzed as in (B). T, total lysate (2.5%); UB, unbound protein (2.5%); B, bound protein (100%). The arrowhead indicates degradation products of Por1-3xHA. The asterisk indicates a cross reaction of the anti-Om45 antibody. **(I)** The contact site formed by Cqd1 and Om14 is independent of MICOS. Mitochondria of wild type, Om14-3×HA and Δ*mic60* Om14-3×HA strains were analyzed as in (B). T, total lysate (1%); UB, unbound protein (1%); B, bound protein (100%). The asterisk indicates a cross reaction of the anti-Mic60 antibody.

330 These two crosslink products of about 80 and 100 kDa indicated interaction partners with a molecular
331 weight of about 15 and 30 kDa. We identified Om14 and Por1, two highly abundant proteins forming
332 a complex in the mitochondrial outer membrane (Lauffer et al., 2012; Sakaue et al., 2019; Wenz et al.,
333 2014), as promising candidates. Consistently, immunoprecipitation of Om14-3xHA allowed the co-
334 isolation of Cqd1 and Por1 (Fig. 6G) and Cqd1 was co-isolated upon immunoprecipitation of Por1-3xHA
335 (Fig. 6H). The co-isolation efficiency of Cqd1 was even higher than the co-isolation efficiency of Om45,
336 a previously identified interaction partner of Por1 in the outer membrane (Lauffer et al., 2012; Sakaue
337 et al., 2019; Wenz et al., 2014). Of note, we were not able to co-purify Por1 by isolating Cqd1-3xHA
338 (Fig. 6B) indicating that immunoprecipitation of Cqd1 impacts the integrity of the complex.

339 Most of the so far identified contact sites between the mitochondrial inner and outer membranes
340 depend on MICOS (Bohnert et al., 2012; Darshi et al., 2011; Harner et al., 2011; Hoppins et al., 2011;
341 Korner et al., 2012; Modi et al., 2019; von der Malsburg et al., 2011; Xie et al., 2007; Zerbes et al.,
342 2012). In particular, Mic60 is essential for the integrity of the MICOS complex as well as the formation
343 of MICOS-dependent contact sites (Harner et al., 2011; Hoppins et al., 2011; von der Malsburg et al.,
344 2011). Although we did not detect a physical interaction between Cqd1 and MICOS, the interaction of
345 Cqd1 with Por1 and Om14 might still depend on the presence of intact MICOS complex. To test this,
346 we performed immunoprecipitation of Om14-3xHA expressed in the wild type background or the
347 Δ*mic60* deletion background. We observed that immunoprecipitation of Om14-3xHA led to the
348 successful co-isolation of Cqd1 and Por1 independent of the presence of Mic60 (Fig. 6I).
349 Taken together, we identified a novel contact site formed by the mitochondrial inner membrane
350 protein Cqd1 and the previously described Por1-Om14 complex in the mitochondrial outer membrane
351 (Lauffer et al., 2012; Sakaue et al., 2019). This new contact site exists independent of contact sites
352 formed by MICOS.
353
354 **Overexpression of *CQD1* leads to altered mitochondrial architecture and morphology**
355 Cells overexpressing *CQD1* from the strong *GAL* promoter showed a dramatically reduced growth rate
356 (Fig. 7A). Western Blot analysis using a Cqd1 specific antibody revealed the appearance of a slower
357 migrating band, probably representing the accumulation of some Cqd1 precursor protein, upon
358 overexpression (Fig. 7A, arrowhead). However, the levels of several other mitochondrial proteins
359 involved in mitochondrial dynamics, protein import, mitochondrial architecture or respiration were
360 not changed compared to wild type and the Δ*cqd1* deletion mutant (Fig. 7B). Even though Mic10 and
361 Mic60 were present at wild type levels (Fig. 7B), we observed that assembled MICOS complex was
362 virtually absent when *CQD1* was overexpressed (Fig. 7C). Similarly, monomeric and dimeric F_1F_O ATP
363 synthase complexes were strongly reduced. In contrast, respiratory chain super complexes were not
364 significantly changed (Fig. 7C).
365 MICOS and the F_1F_O ATP synthase are essential for the establishment of mitochondrial inner membrane
366 architecture (Klecker and Westermann, 2021). MICOS is responsible for the generation and
367 maintenance of crista junctions and deletion of its core subunits Mic10 and Mic60 leads to the
368 formation of internal membrane vesicles without connection to the inner boundary membrane
369 (Alkhaja et al., 2012; Harner et al., 2011; Head et al., 2011; Hoppins et al., 2011; John et al., 2005; Rabl
370 et al., 2009; von der Malsburg et al., 2011). Absence of assembled, dimeric F_1F_O ATP synthase results
371 in the formation of septa that cross the matrix completely or onion-like inner membrane structures
372 (Davies et al., 2012; Habersetzer et al., 2013; Harner et al., 2016; Hoppins et al., 2011; Paumard et al.,
373 2002; Rabl et al., 2009; Strauss et al., 2008). Therefore, we asked whether the lack of assembled MICOS

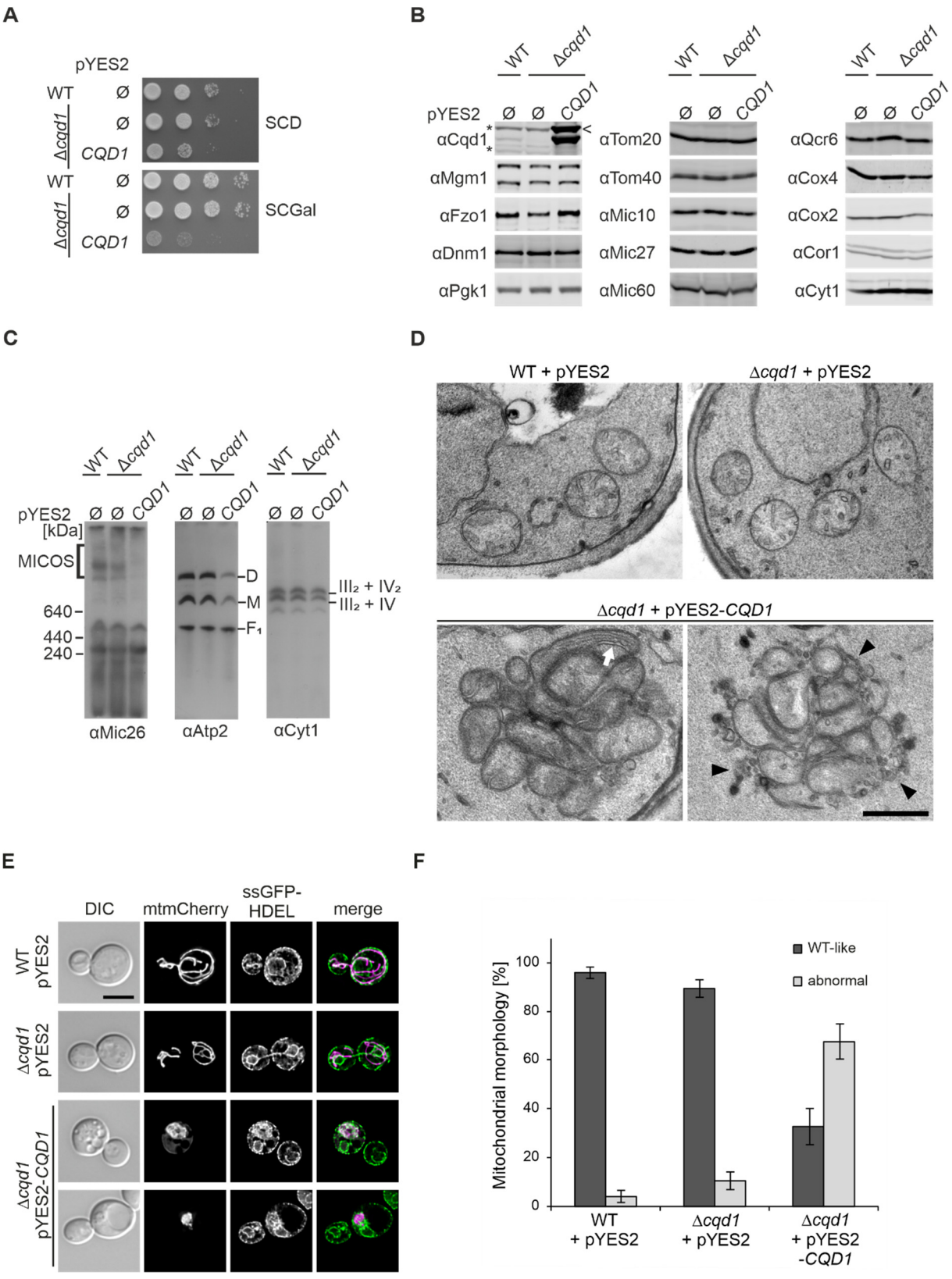
A
pYES2
WT
Δcqd1
Ø
Ø
CQD1
SCD
SCGal
B
WT
Δcqd1
pYES2
Ø
CQD1
αCqd1
αMgm1
αFzo1
αDnm1
αPgk1
αTom20
αTom40
αMic10
αMic27
αMic60
αQcr6
αCox4
αCox2
αCor1
αCyt1
C
[kDa]
MICOS
640
440
240
D
III₂ + IV₂
III₂ + IV
αMic26
αAtp2
αCyt1
WT + pYES2
Δcqd1 + pYES2
Δcqd1 + pYES2-CQD1
E
DIC
mtmCherry
ssGFP-HDEL
merge
WT pYES2
Δcqd1 pYES2
Δcqd1 pYES2-CQD1
F
WT-like
abnormal
Mitochondrial morphology [%]
100
80
60
40
20
0
WT + pYES2
Δcqd1 + pYES2
Δcqd1 + pYES2 -CQD1

Figure 7. Overexpression of *CQD1* leads to dramatic changes in architecture and morphology of mitochondria.

(A) Overexpression of *CQD1* is toxic. Wild type and Δ*cqd1* cells carrying an empty vector (pYES2) and Δ*cqd1* cells expressing *CQD1* from a high-copy plasmid with a galactose-inducible promoter (pYES2-*CQD1*) were grown in synthetic complete medium containing glucose (SCD) or galactose (SCGal) and growth was analyzed by drop dilution assay at 30°C. **(B)** Deletion or overexpression of *CQD1* does not affect steady state levels of mitochondrial proteins. Whole cell extracts of wild type and yeast cells in which *CQD1* was deleted or overexpressed were analyzed by immunoblotting. Asterisks indicate cross reactions of the anti-Cqd1 antibody. The arrowhead indicates the potential precursor form of Cqd1. **(C)** Overexpression of Cqd1 results in strongly reduced levels of assembled MICOS and F_1F_O ATP synthase. Isolated mitochondria of cells grown in SCGal were lysed in buffer containing digitonin (3% w/v) and cleared lysates were subjected to BN-PAGE. The assembly of MICOS, the F_1F_O ATP synthase or the respiratory chain super complexes was analyzed by immunoblotting using antibodies against Mic26, Atp2 or Cyt1. D, dimer of the F_1F_O ATP synthase; M, monomer of the F_1F_O ATP synthase; F_1, F_1 subcomplex of the F_1F_O ATP synthase. **(D)** Overexpression of *CQD1* results in highly altered mitochondrial architecture. Cells were grown overnight in SCGal, subjected to chemical fixation with glutaraldehyde and osmium tetroxide, embedded in Epon, and ultrathin sections were analyzed by transmission electron microscopy. The white arrow highlights sheet-like inner membrane structures, black arrowheads highlight membranes presumably representing cross-sections of ER tubules. Scale bar, 500 nm. Additional electron micrographs are shown in Suppl. Fig. 2. **(E)** Overexpression of *CQD1* leads to the formation of mitochondria-ER clusters. Strains expressing mitochondria-targeted mCherry (mtmCherry) and ER-targeted GFP (ssGFP-HDEL) were grown to logarithmic growth phase in SCGal, fixed with formaldehyde, and examined by deconvolution fluorescence microscopy. Shown are maximum intensity projections of z stacks of entire cells (mitochondria) or of the center of the cells (ER, four consecutive z sections). DIC, *differential interference contrast.* Scale bar, 5 µm. **(F)** Strains expressing mitochondria-targeted GFP were analyzed as in (E) and mitochondrial morphology was quantified. Columns represent mean values from two independent experiments with three biological replicates per strain and at least 150 cells per replicate, error bars indicate standard deviation. Representative images are shown in Suppl. Fig. 3.

409 and F_1F_O ATP synthase complexes in the *CQD1* overexpression strain results in altered mitochondrial
410 architecture. The Δ*cqd1* deletion strain appeared wild type like in electron micrographs, whereas
411 overexpression of *CQD1* led to massively distorted mitochondrial membrane architecture in many cells
412 (Fig. 7D, Suppl. Fig. 2). Mitochondria were often aggregated into huge clusters and we frequently
413 observed loss of normal cristae, often accompanied by the formation of septa and elongated inner
414 membrane structures (Fig. 7D, arrow, Suppl. Fig. 2). Thus, aberrant mitochondrial ultrastructure upon
415 overexpression of Cqd1 complements the loss of assembled MICOS and F_1F_O ATP synthase.
416 Furthermore, in several cases we noticed membraneous structures within these clusters that might
417 represent ER membranes (Fig. 7D, arrowheads, Suppl. Fig. 2). To test this, we simultaneously analyzed
418 the morphology of mitochondria and the ER by fluorescence microscopy in wild type and the *CQD1*
419 deletion and overexpression strains. When *CQD1* was overexpressed mitochondria in most cells did
420 not appear as the characteristic tubular network that is spread all over the cell, but instead formed
421 swollen clusters (Fig. 7E and F, Suppl. Fig. 3). Strikingly, these clusters indeed contained a large
422 proportion of ER membranes (Fig. 7E) pointing to a possible role of Cqd1 in the establishment of
423 mitochondrial ER contacts.

424 In summary, overexpression of Cqd1 causes severe phenotypes on growth, formation of mitochondrial
425 structural elements, and mitochondrial architecture and morphology. Interestingly, the effect of
426 overexpression of the inner membrane protein Cqd1 is apparently not only restricted to the inner
427 membrane but also affects inter-organellar contacts. Therefore, we conclude that the Cqd1-Por1-
428 Om14 contact site is important for cellular membrane organization in addition to its role in the
429 phospholipid and coenzyme Q metabolism.
430

431 ## Discussion

432 In the present study, we characterized the highly conserved protein kinase-like domain containing
433 protein Cqd1. All members of the UbiB family present in yeast, Cqd1, Cqd2 and Coq8, participate in
434 coenzyme Q metabolism (Do et al., 2001; Johnson et al., 2005; Kemmerer et al., 2021; Reidenbach et
435 al., 2018; Stefely et al., 2015; Subramanian et al., 2019; Xie et al., 2012). In contrast to the Δ*coq8*
436 mutant deletion of *CQD1* does not result in reduced production but affects distribution of coenzyme
437 Q within the cellular membrane system (Kemmerer et al., 2021). The molecular role of Cqd1 in this
438 process is unknown so far. However, membrane contacts would be ideally suited to facilitate the
439 transition of these hydrophobic molecules (Kemmerer et al., 2021). These contacts would have to be
440 present between the mitochondrial inner membrane and the outer membrane as well as between the
441 outer membrane and other organelles. Key findings obtained in our study are in good agreement with
442 this hypothesis: (i) The inner membrane protein Cqd1 forms a contact site with the Por1-Om14
443 complex in the outer membrane; (ii) the level of Cqd1 influences the interaction between mitochondria
444 and the ER; (iii) Cqd1 modulates the architecture and the morphology of mitochondria; and (iv) Cqd1
445 is important for mitochondrial phospholipid homeostasis in addition to its role in coenzyme Q
446 distribution.
447 Based on these results we propose that Cqd1 exerts its function as a key component of a novel
448 membrane contact site. Its interaction with Om14 and Por1 places Cqd1 in an ideal position to control
449 the distribution of coenzyme Q produced in the inner membrane to the outer membrane and then
450 further to the cellular endomembrane system. Similarly, it might coordinate the import of phosphatidic
451 acid, and possibly other lipids, from the ER into the inner membrane. We consider it unlikely that Cqd1
452 itself is a lipid transporter, as the absence of Cqd1 leads to increased export of coenzyme Q rather than
453 block of transport (Kemmerer et al., 2021). Instead it is conceivable that Cqd1 has an accessory or
454 regulatory role and interacts with additional, yet unknown interaction partners in the inner membrane.
455 This idea would be in line with models of other lipid transport systems, like the bacterial maintenance
456 of lipid asymmetry (Mla) pathway first identified in *E. coli* (Malinverni and Silhavy, 2009). Here the
457 MlaFEDB complex is involved in the ATP-dependent transport of lipids between the bacterial inner and

458 outer membranes (Malinverni and Silhavy, 2009; Thong et al., 2016). This complex is composed of the
459 canonical proteins MlaE and MlaF and the auxiliary proteins MlaB and the hexameric MlaD in the inner
460 membrane, and cooperates with MlaC, a soluble protein in the periplasm, and the outer membrane
461 protein MlaA (Ekiert et al., 2017; Malinverni and Silhavy, 2009; Thong et al., 2016). Intriguingly, MlaA
462 interacts with the porins OmpC and OmpF (Chong et al., 2015) and it was proposed that it works in
463 both directions between the bacterial membranes (Ekiert et al., 2017; Malinverni and Silhavy, 2009).
464 Thus, it shares two features with Cqd1: an interaction with porin across two membranes and the
465 regulation of bi-directional lipid transport.
466 While Gram-negative bacteria distribute lipids only between two membranes, mitochondria in
467 addition exchange lipids with the ER and other organelles. About ten years ago the presence of an ER–
468 mitochondria organizing network called ERMIONE was proposed. It was suggested that a continuum
469 exists that connects the mitochondrial inner membrane through MICOS with the ER to facilitate the
470 flux of calcium and the transport of lipids (van der Laan et al., 2012). Interestingly, the interaction of
471 MICOS and Miro1 and Miro2 has been shown in mammalian cells recently (Modi et al., 2019). Miro
472 GTPases are the mammalian orthologs of the yeast ER-mitochondria encounter structure (ERMES)
473 subunit Gem1. Similar to ERMES, Miro1 and 2 are present in Endoplasmic Reticulum-Mitochondria
474 Contacts Sites (ERMCS) (Modi et al., 2019). Thus, the interaction of MICOS and the Miro GTPases might
475 represent a part of the previously proposed ERMIONE in mammals (van der Laan et al., 2012).
476 Interestingly, a recent study using yeast as model organism shows that ERMES is important for the
477 assembly of MICOS and that both complexes co-localize indicating the existence of ERMIONE also in
478 yeast (Tirrell et al., 2020). However, it is plausible that additional complexes might exist that participate
479 in the ER–mitochondria organizing network. Intriguingly, Por1 was shown to interact with ER proteins
480 in yeast and mammals (Geva et al., 2017; Kornmann et al., 2011; Murley et al., 2015; Xu et al., 2018).
481 Therefore, Cqd1 might modulate membrane organization by regulating inter-organellar contacts
482 formed by Por1. Consistently, we observed dramatically increased mitochondria-ER interactions upon
483 Cqd1 overexpression.
484 Overexpression of Cqd1 also results in altered mitochondrial architecture. These changes are often
485 accompanied by the formation of septa and aberrant inner membrane structures. We and others
486 observed similar phenotypes when analyzing yeast mutants lacking MICOS or dimeric F_1F_O ATP
487 synthase (Alkhaja et al., 2012; Davies et al., 2012; Harner et al., 2011; Head et al., 2011; Hoppins et al.,
488 2011; John et al., 2005; Paumard et al., 2002; Rabl et al., 2009; von der Malsburg et al., 2011). And
489 indeed, overexpression of *CQD1* goes along with a strong reduction of assembled MICOS complex and
490 F_1F_O ATP synthase. This is particularly interesting as the steady state level of the MICOS core subunits
491 Mic10 and Mic60, that are essential for its integrity, are normal in the Cqd1 overexpression mutant.
492 This indicates that Cqd1 has a function in mitochondrial architecture that goes beyond regulation of

493 coenzyme Q and phosphatidic acid homeostasis. It remains a challenge for the future to reveal the
494 molecular mechanisms in this process.
495

496 ## Material and Methods

497 **Yeast strains and cell growth**

498 *S. cerevisiae* YPH499 was used as wild type (WT). Chromosomal manipulations (knockouts, C-terminal
499 3xHA and 3xMyc tagging) were performed according to established procedures (Knop et al., 1999;
500 Longtine et al., 1998). For the generation of deletion strains, the entire coding regions of the
501 corresponding genes were replaced by the indicated marker cassettes. Double mutant strains were
502 also generated by homologous recombination. The genotypes of the strains used in this study are listed
503 in Supplementary Table 2.
504 For the generation of pRS316-*CQD1,* pRS316-*CQD1*-3xHA and pYES2-*CQD1* plasmids, the coding region
505 of *CQD1* was amplified by PCR. The intron present in the *CQD1* open reading frame was removed when
506 cloning the initial pYES2 construct. This construct served as template DNA for cloning of pRS316-*CQD1*.
507 The coding region of *CQD1*-3xHA was amplified from yeast genomic DNA of the *CQD1*-3xHA strain.
508 *CQD1*-3xHA was cloned under control of its endogenous promoter and the *ADH1* terminator into the
509 pRS316 vector by enzymatic assembly of overlapping DNA fragments (Gibson, 2011). The point
510 mutations K275A, D288A, and E330A in *CQD1* were introduced into pRS316-*CQD1* by site directed
511 mutagenesis. For the generation of the pYX142-ssGFP-HDEL plasmid the *Sac*I/*Eco*RI fragment of
512 pYX122-ssGFP-HDEL (Bockler and Westermann, 2014) was ligated into the *Sac*I/*Eco*RI sites of pYX142-
513 mtGFP (Westermann and Neupert, 2000). The primers used in this study are listed in Supplementary
514 Table 3.
515 Yeast cells were grown as indicated on YP medium supplemented with 2% glucose (YPD) or 3% glycerol
516 (YPG) or synthetic medium supplemented with 2% glucose (SCD), 3% galactose (SCGal) or 3% glycerol
517 (SCG) (Izawa and Unger, 2017).
518 Growth of the different strains was analyzed by the drop dilution assay. Cells were grown in YPD liquid
519 medium for 16 h. Cells were kept in logarithmic growth phase, washed with water, diluted in water to
520 an OD_{600} of 0.5 and serial dilutions were prepared (1:10; 1:100; 1:1,000). 5 µl of each dilution were
521 spotted on agar plates with the indicated media. For analysis of cell growth on YP medium, cells were
522 harvested after growth in YPD. All remaining analyses were done on synthetic medium. Here, cells
523 were shifted from YPD to SCD 30 h prior to analysis.
524

525 **Whole cell extract**

526 Cells were grown in the indicated media to exponential growth phase (OD_{600} 0.5 - 1.0) and an
527 equivalent of cells corresponding to 2.5 OD_{600} was collected by centrifugation. Harvested cells were
528 resuspended in 200 µl of 0.1 M NaOH and incubated at room temperature for 5 min. Cell pellets were
529 resuspended in 50 µl of SDS sample buffer and analyzed by SDS-PAGE and immunoblotting.

530

531 **Isolation of crude mitochondria**

532 Cells were grown at 30°C on SCD, SCG, SCGal or YPG as indicated. Mitochondria were isolated by
533 differential centrifugation as described previously (Izawa and Unger, 2017) with slight modifications.
534 In brief, cells were harvested and washed with distilled water. Cells were treated for 10 min with DTT
535 (10 mM final concentration) followed by treatment with zymolyase (200 U per gram wet weight of
536 cells) for 30 min at 30°C with gentle agitation. Sphaeroplasts were opened by repeated pipetting in
537 isotonic lysis buffer (20 mM MOPS-KOH pH 7.2, 1 mM EDTA, 0.6 M sorbitol, 0.2% (w/v) BSA, 1 mM
538 phenylmethylsulfonyl fluoride (PMSF)). Mitochondria were harvested after a clarifying spin at 2,000 ×g
539 and 4°C for 5 min by centrifugation at 14,000 ×g and 4°C for 10 min and resuspended in SM buffer (0.6
540 M sorbitol, 20 mM MOPS, pH 7.4).

541

542 **Sucrose gradient purification of mitochondria**

543 Crude mitochondria were isolated as described above except that the final mitochondrial pellet was
544 resuspended in 15 ml of buffer A (0.6 M Sorbitol, 50 mM MES pH 6.0) and re-isolated by centrifugation
545 for 10 min at 17,000 xg and 4°C. Crude mitochondria were resuspended in 2 ml of buffer A and 10 mg
546 were loaded on top of a sucrose step gradient (1.5 ml of 60%, 5 ml of 35%, 1.5 ml of 25%, and 1.5 ml
547 of 15% sucrose in buffer A). Mitochondria were separated from other organelles by ultracentrifugation
548 for 1 h at 134,000 xg and 4°C. Purified mitochondria were harvested from the boundary between 60%
549 and 35% sucrose layers, resuspended in 15 ml of SM buffer and re-isolated by centrifugation for 15
550 min at 14,000 xg and 4°C. Mitochondria were resuspended in SM buffer to a final concentration of 10
551 mg/ml.

552

553 **Subfractionation of mitochondria**

554 Vesicles consisting of pure mitochondrial outer membrane, mitochondrial inner membrane, and
555 vesicles consisting of both membranes were generated and separated as described before (Harner,
556 2017) with slight modifications. 10 mg of freshly isolated crude mitochondria were resuspended in 1.6
557 ml of SM buffer. Mitochondria were swollen by addition of 16 ml swelling buffer (20 mM MOPS pH
558 7.4) and subsequent incubation for 30 min at 4°C under mild stirring. Sucrose concentration was
559 adjusted to 0.55 M. Vesicles were generated by sonication (four times 30 seconds at 10% amplitude

560 intermitted by 30 seconds breaks). After a clarifying spin for 20 min at 20,000 ×g and 4°C, vesicles were
561 concentrated on the 2.5 M sucrose cushion by centrifugation at 118,000 ×g and 4°C for 100 min.
562 Concentrated vesicles were harvested and the suspension was homogenized by dounce
563 homogenization. Vesicles were separated by centrifugation for 12 hours at 200,000 ×g and 4°C through
564 a sucrose step gradient (0.8 M, 0.96 M, 1.02 M, 1.13 M, 1.25 M sucrose in 20 mM MOPS-KOH pH 7.4
565 and 0.5 mM EDTA). The gradient was harvested and proteins were subjected twice to trichloroacetic
566 acid precipitation (TCA; final concentration of 14.4%).
567
568 **Alkaline extraction**
569 100 µg of isolated mitochondria were diluted in SM buffer to a concentration of 1 mg/ml. An equal
570 volume of 200 mM sodium carbonate was added followed by an incubation on ice for 30 min.
571 Membrane and soluble proteins were separated by centrifugation for 30 min at 91,000 ×g and 4°C.
572 Proteins present in the supernatant were subjected to TCA precipitation. The membrane protein pellet
573 and the precipitated soluble proteins were resuspended in SDS sample buffer and analyzed by SDS-
574 PAGE and immunoblotting.
575
576 **Proteolytic susceptibility assay**
577 100 µg of mitochondria were incubated in SM buffer (0.6 M sorbitol, 20 mM MOPS, pH 7.4), swelling
578 buffer (20 mM MOPS, pH 7.4) or lysis buffer (1% (v/v) Triton X-100, 20 mM MOPS, pH 7.4) for 20 min
579 on ice. Proteinase K was added (final concentration of 0.2 mg/ml) as indicated and samples were
580 incubated on ice for 15 min. Proteolysis was stopped by addition of PMSF to a final concentration of 4
581 mM. Samples were centrifuged at 17,000 ×g and 4°C for 20 min. Pellets were resuspended in SM buffer
582 and subjected to TCA precipitation. Samples were analyzed by SDS-PAGE and immunoblotting.
583
584 **Blue native gel electrophoresis (BN-PAGE**)
585 150 µg (MICOS complex) or 50 µg (all other mitochondrial protein complexes) of isolated mitochondria
586 were resuspended in 15 µl (MICOS complex) or 50 µl (all other mitochondrial protein complexes) of
587 BN buffer (50 mM NaCl, 50 mM imidazole-HCl, 2 mM 6-aminohexanoic acid, 1 mM EDTA, 1 mM PMSF,
588 pH 7.0) (Wittig et al., 2006) supplemented with 3% digitonin. After a clarifying spin for 15 min at 14,000
589 ×g and 4°C 2 µl (MICOS complex) or 7 µl (all other mitochondrial protein complexes) G-250 Sample
590 Additive (Invitrogen, Waltham, Massachusetts, USA) containing 40% glycerol were added. Protein
591 complexes were separated on 3-12% NativePAGE Novex Bis-Tris gels (Invitrogen). Electrophoresis was
592 performed for 30 min at 150 V followed by 2 hours at 250 V. Proteins were transferred to PVDF
593 membrane by wet blotting for 2 hours at 30 mV.

594 **Chemical crosslinking**

595 Isolated mitochondria were diluted in 100 µl of SI buffer (50 mM HEPES-KOH, 0.6 M sorbitol, 75 mM
596 KCl, 10 mM $Mg(Ac)_2$, 2 mM KH_2PO_4, 2.5 mM EDTA, 2.5 mM $MnCl_2$, pH 7.2) to a concentration of 1
597 mg/ml. Disuccinimidyl glutarate (DSG) and m-maleimidobenzoyl-N-hydroxysuccinimide ester (MBS)
598 were added from freshly prepared stock solutions to the final concentration of 200 or 400 µM and
599 incubated on ice for 30 min. The reaction was stopped by the addition of glycine to a final
600 concentration of 100 mM followed by incubation on ice for 10 min. Mitochondria were re-isolated by
601 centrifugation at 17,000 xg and 4°C for 10 min. The pellets were resuspended in SDS sample buffer and
602 analyzed by SDS-PAGE and immunoblotting.

603

604 **Immunoprecipitation assay**

605 3 mg mitochondria (except for Cqd1-3×HA, 1 mg of mitochondria) were lysed in IP buffer (50 mM Tris-
606 HCl pH 7.4, 50 mM NaCl) containing 1% (w/v) digitonin and 1 mM PMSF. After a clarifying spin for 10
607 min at 12,000 xg and 4°C, lysates were incubated with anti-HA agarose beads (20 µl of beads per 1 mg
608 of proteins) (Merck, Darmstadt, Germany) for 2 h. Anti-HA agarose beads were washed 3 times with
609 500 µl IP buffer containing 0.1% (w/v) digitonin and 1 mM PMSF before and after incubation with
610 lysates. The indicated amount of total lysate and unbound material was taken, subjected to TCA
611 precipitation and resuspended in SDS sample buffer. Bound proteins were eluted with SDS sample
612 buffer at 95°C for 10 min. Fractions were analyzed by SDS-PAGE followed by immunoblotting.

613

614 **Fluorescence microscopy**

615 For visualizing mitochondria, the mitochondrial presequence of *Neurospora crassa* subunit 9 of the
616 F_1F_O ATP synthase was fused to mKate2. The nucleotide sequence was inserted into the HO locus of
617 the yeast genome and expressed constitutively under the control of the *PGK1* promoter. Yeast cells
618 were grown overnight in YPD at 30°C. The next day, cells were diluted in synthetic media containing
619 2% glucose and were kept in logarithmic phase for 24 hours. Cells corresponding to an OD_{600} of 1 were
620 harvested by centrifugation at 2,500 xg for 3 min. Cells were vortexed for 1 min and washed with 1 ml
621 of sterile 1x PBS. Cell pellets were resuspended in 200 µl 1x PBS and immobilized on µ-slides (Ibidi,
622 Gräfelfing, Germany) coated with 1 mg/ml of concanavalin A. After immobilizing, cells were covered
623 with 400 µl SCD medium. Microscopy was performed at 30°C on a Nikon Ti2-Eclipse microscope (Nikon,
624 Tokyo, Japan) equipped with a CFI Apochromat TIRF 100x/1.49 NA oil objective and a TwinCam LS dual
625 camera splitter attached to two Photometrics Prime 95B 25 mm cameras (Teledyne Photometrics,
626 Tucson, USA).

627 For visualization of mitochondria or mitochondria and the ER upon *CQD1* overexpression, strains
628 carried either pYX142-mtGFP (Westermann and Neupert, 2000) or pYX232-mtmCherry (Dirk Scholz,
629 University of Bayreuth) and pYX142-ssGFP-HDEL, respectively. Cells were grown overnight in
630 galactose-containing synthetic complete medium supplemented with 0.1% glucose, shifted to
631 galactose-containing synthetic complete medium without glucose, incubated until logarithmic growth
632 phase and fixed with 3.7% formaldehyde. Microscopy was performed using a Leica DMi8 fluorescence
633 microscope (Leica Microsystems GmbH, Wetzlar, Germany) equipped with a HC PL APO 100x/1.40 oil
634 objective, a Lumencor SPECTRA X light source and fluorescence filter sets (TXR Cube ex. 540-580 nm;
635 em. 592-668 nm and FITC Cube ex. 460-500 nm; em. 512-542 nm). Images were taken with a Leica
636 DFC9000 GT VSC-07400 sCMOS camera. For microscope settings, image generation, and processing
637 (cropping, maximum intensity projection), the Leica LAS X software (version 3.6.0.20104, Leica
638 Microsystems GmbH, Wetzlar, Germany) was used. For deconvolution of z stacks the Deconvolution
639 Software Huygens Essential (version 18.10, Scientific Volume Imaging, Hilversum, The Netherlands)
640 was used. For adjustment of brightness and contrast and the overlay of different channels Adobe
641 Photoshop CS6 (Adobe Systems) was used. For simultaneous analysis of the morphology of
642 mitochondria and the ER, z stacks were recorded with a z-step size of 213 nm. In the case of
643 mitochondria, maximum intensity projections of z stacks of entire cells are shown, whereas for the ER
644 maximum intensity projections of four consecutive z sections of the center of the cells are shown.
645
646 **Electron microscopy**
647 For electron microscopy, cells were first grown in synthetic complete medium containing glucose as
648 carbon source and then shifted to synthetic complete medium containing galactose as carbon source,
649 in which they were grown overnight. Chemical fixation of yeast cells with glutaraldehyde and osmium
650 tetroxide, dehydration, Epon embedding, and subsequent steps of sample preparation for electron
651 microscopy were performed as described previously (Unger et al., 2017). Electron micrographs were
652 taken with a JEOL JEM-1400 Plus transmission electron microscope operated at 80 kV, a JEOL Ruby
653 CCD camera (3296 x 2472 pixels), and the TEM Center software Ver.1.7.12.1984 or Ver.1.7.19.2439
654 (JEOL, Tokyo, Japan).
655
656 **Lipid analysis**
657 Lipidomics analyses were performed as described in Papagiannidis et al. (2021) . Aliquots
658 corresponding to 1500-2000 pmol total lipid were subjected to acidic Bligh and Dyer extractions
659 performed in the presence of internal lipid standards from a master mix containing 40 pmol d_7-PC mix
660 (15:0/18:1-d7, Avanti Polar Lipids), 25 pmol PI (17:0/20:4, Avanti Polar Lipids), 25 pmol PE and 15 pmol
661 PS (14:1/14:1, 20:1/20:1, 22:1/22:1, semi-synthesized as described in Özbalci et al, 2013), 20 pmol PA

662 (PA 17:0/20:4, Avanti Polar Lipids) 5 pmol PG (14:1/14:1, 20:1/20:1, 22:1/22:1, semi-synthesized as
663 described in Ozbalci et al. (2013) , 25 pmol CL 57:4 (14:1/14:1/14:1/15:1, Avanti Polar Lipids) and 25
664 pmol MLCL (16:0/16:0/16:0, Echelon). Lipids recovered in the organic extraction phase were
665 evaporated by a gentle stream of nitrogen. Prior to measurements, lipid extracts were dissolved in 10
666 mM ammonium acetate in methanol, diluted 1:10 and transferred into Eppendorf twin.tec 96-well
667 plates. Mass spectrometric measurements were performed in positive ion mode on an AB SCIEX QTRAP
668 6500+ mass spectrometer equipped with chip-based (HD-D ESI Chip, Advion Biosciences) nano-
669 electrospray infusion and ionization (Triversa Nanomate, Advion Biosciences) as described (Özbalci et
670 al, 2013). The following precursor ion scanning (PREC) and neutral loss scanning (NL) modes were used
671 for the measurement of the various lipid classes: +PREC 184 (PC), +NL141 (PE), +NL185 (PS), +NL277
672 (PI), +NL189 (PG), +NL115 (PA). Mass spectrometry settings: Resolution: unit, low mass configuration;
673 data accumulation: 400 MCA; curtain gas: 20; interface heater temperature: 60°C; CAD: medium. Data
674 evaluation was done using LipidView (Sciex) and ShinyLipids, a software developed in house. For MS
675 analysis of CL and MLCL, dried lipids were re-dissolved in 40% UPLC solvent B (90% 2-propanol/10%
676 acetonitrile/0.1% formic acid/10 mM NH_4HCO_3) and transferred to silanized glass inserts
677 (Phenomenex) using Hamilton syringes. The glass inserts were placed in Eppendorf tubes and
678 centrifuged in an Eppendorf centrifuge at 3000 rpm for 3 min. Lipid samples were then subjected to
679 UPLC-ESI-MS/MS analysis performed on an Ultimate® 3000 LC system (Dionex, Thermo Fisher
680 Scientific) coupled to a QExactive Hybrid Quadrupole-Orbitrap instrument (Thermo Scientific). For LC
681 separations, an ACQUITY UPLC CSH C18 1.7µm, 1.0 x 150 mm column (Waters) was used. The column
682 oven temperature was set to 55°C, the temperature of the autosampler was set to 20°C. The flow rate
683 used was 100 µl/min. The solvent composition used was as follows: 60% acetonitrile/40% H_2O/0.1%
684 formic acid/10 mM NH_4HCO_3 (solvent A), 90% 2-propanol/10% acetonitrile/0.1% formic acid/10 mM
685 NH_4HCO_2 (solvent B). The starting solvent composition was 50% solvent B/50% solvent A. The
686 conditions of the gradient were as follows: 7 min: 90% solvent B, 7-17 min: 90% solvent B, 17.1 min
687 50% solvent B and 17.1-25 min: 50% solvent B. The MS analyses were performed in the positive ion
688 mode. CL and MLCL species were measured as $[M+NH_4^+]$ ions. The following ESI source parameters
689 were used: sheath gas flow rate: 4 (a.u.), auxiliary gas flow rate: 0, sweep gas flow rate: 0, spray
690 voltage: 1.5 kV, capillary temperature: 200°C, S-lens RF level: 50. Full-MS scans were recorded using
691 the following parameters: resolution: 140,000 (at m/z 200) AGC-target: 1e6, maximum IT: 200 ms, scan
692 range: m/z 500-2000. Data evaluation was performed using MassMap.
693

694 **Statistics**

695 Statistics were calculated using the software GraphPad Prism (version 5; GraphPad, San Diego, CA,
696 USA). Mass spectrometry analysis was performed in quadruplicate. Data are represented as mean ±
697 standard deviation. For statistical analysis, data was first tested for normal distribution using Shapiro-
698 Wilk normality test. P-Values were calculated using Mann Whitney test. Analysis of Mdj1 precursor
699 accumulation and Mgm1 processing in the various yeast strains was performed in triplicate. Data are

700 represented as mean ± standard deviation. P-Values were calculated using an unpaired Student's t
701 test. $p < 0.05$ was considered statistically significant.

702

703 Acknowledgements

704 M.E.H. thanks the Jung-Stiftung für Wissenschaft und Forschung, the Friedrich-Baur-Stiftung (Reg.-Nr.
705 02-20), *LMUexcellent* and the Deutsche Forschungsgemeinschaft (DFG), project number 413985647
706 for financial support. B.B. was supported by the DFG, project number 112927078 - TRR 83, B.W. was
707 supported by the DFG, project number 433461293, T.K. was supported by the DFG, project number
708 459304237, and the Elitenetzwerk Bayern (ENB) through the Biological Physics program. We thank Rita
709 Grotjahn (University of Bayreuth) for help with electron microscopy. We acknowledge the donation of
710 the Sec61 antibody by Dr. Tom Rapoport, Harvard Medical School, Cambridge. M.E.H. thanks Dr.
711 Christof Osman, Ludwig-Maximilians University, Munich, for providing his microscope and support.
712 M.E.H. is greatly thankful for the helpful discussion with Dr. Bill Wickner, Dartmouth Medical School,
713 Hanover. Furthermore, M.E.H. thanks Dr. Michael Kiebler, Ludwig-Maximilians, University, Munich, for
714 generous and extensive support.

715

716 Conflict of interest

717 The authors declare that there is no conflict of interest.

718

719 Author contributions

720 S.K., X.C., A.K.U, T.K., M.E.H., conception and design, acquisition of data, analysis and interpretation of
721 data, drafting or revising the article; T.S., C.L., R.S., acquisition of data, analysis and interpretation of
722 data, revising the article; B.B., B.W., W.N., conception and design, analysis and interpretation of data,
723 drafting or revising the article.

724

725 References

726 Alkhaja, A.K., Jans, D.C., Nikolov, M., Vukotic, M., Lytovchenko, O., Ludewig, F., Schliebs, W., Riedel, D.,
727 Urlaub, H., Jakobs, S*., et al.* (2012). MINOS1 is a conserved component of mitofilin complexes and
728 required for mitochondrial function and cristae organization. Mol Biol Cell *23*, 247-257.
729 Awad, A.M., Nag, A., Pham, N.V.B., Bradley, M.C., Jabassini, N., Nathaniel, J., and Clarke, C.F. (2020).
730 Intragenic suppressor mutations of the COQ8 protein kinase homolog restore coenzyme Q biosynthesis
731 and function in Saccharomyces cerevisiae. PLoS One *15*, e0234192.
732 Beutner, G., Ruck, A., Riede, B., Welte, W., and Brdiczka, D. (1996). Complexes between kinases,
733 mitochondrial porin and adenylate translocator in rat brain resemble the permeability transition pore.
734 FEBS Lett *396*, 189-195.

735 Bockler, S., and Westermann, B. (2014). Mitochondrial ER contacts are crucial for mitophagy in yeast.
736 Dev Cell *28*, 450-458.
737 Bohnert, M., Wenz, L.S., Zerbes, R.M., Horvath, S.E., Stroud, D.A., von der Malsburg, K., Muller, J.M.,
738 Oeljeklaus, S., Perschil, I., Warscheid, B.*, et al.* (2012). Role of mitochondrial inner membrane
739 organizing system in protein biogenesis of the mitochondrial outer membrane. Mol Biol Cell *23*, 3948-
740 3956.
741 Chacinska, A., Rehling, P., Guiard, B., Frazier, A.E., Schulze-Specking, A., Pfanner, N., Voos, W., and
742 Meisinger, C. (2003). Mitochondrial translocation contact sites: separation of dynamic and stabilizing
743 elements in formation of a TOM-TIM-preprotein supercomplex. EMBO J *22*, 5370-5381.
744 Cherry, J.M., Hong, E.L., Amundsen, C., Balakrishnan, R., Binkley, G., Chan, E.T., Christie, K.R., Costanzo,
745 M.C., Dwight, S.S., Engel, S.R.*, et al.* (2012). Saccharomyces Genome Database: the genomics resource
746 of budding yeast. Nucleic Acids Res *40*, D700-705.
747 Chong, Z.S., Woo, W.F., and Chng, S.S. (2015). Osmoporin OmpC forms a complex with MlaA to
748 maintain outer membrane lipid asymmetry in Escherichia coli. Mol Microbiol *98*, 1133-1146.
749 Claros, M.G., and Vincens, P. (1996). Computational method to predict mitochondrially imported
750 proteins and their targeting sequences. Eur J Biochem *241*, 779-786.
751 Connerth, M., Tatsuta, T., Haag, M., Klecker, T., Westermann, B., and Langer, T. (2012).
752 Intramitochondrial transport of phosphatidic acid in yeast by a lipid transfer protein. Science *338*, 815-
753 818.
754 Costanzo, M., VanderSluis, B., Koch, E.N., Baryshnikova, A., Pons, C., Tan, G., Wang, W., Usaj, M.,
755 Hanchard, J., Lee, S.D.*, et al.* (2016). A global genetic interaction network maps a wiring diagram of
756 cellular function. Science *353*.
757 Darshi, M., Mendiola, V.L., Mackey, M.R., Murphy, A.N., Koller, A., Perkins, G.A., Ellisman, M.H., and
758 Taylor, S.S. (2011). ChChd3, an inner mitochondrial membrane protein, is essential for maintaining
759 crista integrity and mitochondrial function. J Biol Chem *286*, 2918-2932.
760 Davies, K.M., Anselmi, C., Wittig, I., Faraldo-Gomez, J.D., and Kuhlbrandt, W. (2012). Structure of the
761 yeast F1Fo-ATP synthase dimer and its role in shaping the mitochondrial cristae. Proc Natl Acad Sci U
762 S A *109*, 13602-13607.
763 Dekker, P.J., Martin, F., Maarse, A.C., Bomer, U., Muller, H., Guiard, B., Meijer, M., Rassow, J., and
764 Pfanner, N. (1997). The Tim core complex defines the number of mitochondrial translocation contact
765 sites and can hold arrested preproteins in the absence of matrix Hsp70-Tim44. EMBO J *16*, 5408-5419.
766 DeVay, R.M., Dominguez-Ramirez, L., Lackner, L.L., Hoppins, S., Stahlberg, H., and Nunnari, J. (2009).
767 Coassembly of Mgm1 isoforms requires cardiolipin and mediates mitochondrial inner membrane
768 fusion. J Cell Biol *186*, 793-803.
769 Do, T.Q., Hsu, A.Y., Jonassen, T., Lee, P.T., and Clarke, C.F. (2001). A defect in coenzyme Q biosynthesis
770 is responsible for the respiratory deficiency in Saccharomyces cerevisiae abc1 mutants. J Biol Chem
771 *276*, 18161-18168.
772 Eiyama, A., Aaltonen, M.J., Nolte, H., Tatsuta, T., and Langer, T. (2021). Disturbed intramitochondrial
773 phosphatidic acid transport impairs cellular stress signaling. J Biol Chem *296*, 100335.
774 Ekiert, D.C., Bhabha, G., Isom, G.L., Greenan, G., Ovchinnikov, S., Henderson, I.R., Cox, J.S., and Vale,
775 R.D. (2017). Architectures of Lipid Transport Systems for the Bacterial Outer Membrane. Cell *169*, 273-
776 285 e217.
777 Fritz, S., Rapaport, D., Klanner, E., Neupert, W., and Westermann, B. (2001). Connection of the
778 mitochondrial outer and inner membranes by fzo1 is critical for organellar fusion. J Cell Biol *152*, 683-
779 692.
780 Geva, Y., Crissman, J., Arakel, E.C., Gomez-Navarro, N., Chuartzman, S.G., Stahmer, K.R., Schwappach,
781 B., Miller, E.A., and Schuldiner, M. (2017). Two novel effectors of trafficking and maturation of the
782 yeast plasma membrane H(+) -ATPase. Traffic *18*, 672-682.
783 Gibson, D.G. (2011). Enzymatic assembly of overlapping DNA fragments. Methods Enzymol *498*, 349-
784 361.

785 Gonzalez Montoro, A., Auffarth, K., Honscher, C., Bohnert, M., Becker, T., Warscheid, B., Reggiori, F.,
786 van der Laan, M., Frohlich, F., and Ungermann, C. (2018). Vps39 Interacts with Tom40 to Establish One
787 of Two Functionally Distinct Vacuole-Mitochondria Contact Sites. Dev Cell *45*, 621-636 e627.
788 Habersetzer, J., Larrieu, I., Priault, M., Salin, B., Rossignol, R., Brethes, D., and Paumard, P. (2013).
789 Human F1F0 ATP synthase, mitochondrial ultrastructure and OXPHOS impairment: a (super-)complex
790 matter? PLoS One *8*, e75429.
791 Harner, M. (2017). Isolation of Contact Sites Between Inner and Outer Mitochondrial Membranes.
792 Methods Mol Biol *1567*, 43-51.
793 Harner, M., Korner, C., Walther, D., Mokranjac, D., Kaesmacher, J., Welsch, U., Griffith, J., Mann, M.,
794 Reggiori, F., and Neupert, W. (2011). The mitochondrial contact site complex, a determinant of
795 mitochondrial architecture. EMBO J *30*, 4356-4370.
796 Harner, M.E., Unger, A.K., Geerts, W.J., Mari, M., Izawa, T., Stenger, M., Geimer, S., Reggiori, F.,
797 Westermann, B., and Neupert, W. (2016). An evidence based hypothesis on the existence of two
798 pathways of mitochondrial crista formation. Elife *5*.
799 Head, B.P., Zulaika, M., Ryazantsev, S., and van der Bliek, A.M. (2011). A novel mitochondrial outer
800 membrane protein, MOMA-1, that affects cristae morphology in Caenorhabditis elegans. Mol Biol Cell
801 *22*, 831-841.
802 Hoppins, S., Collins, S.R., Cassidy-Stone, A., Hummel, E., Devay, R.M., Lackner, L.L., Westermann, B.,
803 Schuldiner, M., Weissman, J.S., and Nunnari, J. (2011). A mitochondrial-focused genetic interaction
804 map reveals a scaffold-like complex required for inner membrane organization in mitochondria. J Cell
805 Biol *195*, 323-340.
806 Izawa, T., and Unger, A.K. (2017). Isolation of Mitochondria from Saccharomyces cerevisiae. Methods
807 Mol Biol *1567*, 33-42.
808 John, G.B., Shang, Y., Li, L., Renken, C., Mannella, C.A., Selker, J.M., Rangell, L., Bennett, M.J., and Zha,
809 J. (2005). The mitochondrial inner membrane protein mitofilin controls cristae morphology. Mol Biol
810 Cell *16*, 1543-1554.
811 John Peter, A.T., Herrmann, B., Antunes, D., Rapaport, D., Dimmer, K.S., and Kornmann, B. (2017).
812 Vps13-Mcp1 interact at vacuole-mitochondria interfaces and bypass ER-mitochondria contact sites. J
813 Cell Biol *216*, 3219-3229.
814 Johnson, A., Gin, P., Marbois, B.N., Hsieh, E.J., Wu, M., Barros, M.H., Clarke, C.F., and Tzagoloff, A.
815 (2005). COQ9, a new gene required for the biosynthesis of coenzyme Q in Saccharomyces cerevisiae. J
816 Biol Chem *280*, 31397-31404.
817 Kemmerer, Z.A., Robinson, K.P., Schmitz, J.M., Manicki, M., Paulson, B.R., Jochem, A., Hutchins, P.D.,
818 Coon, J.J., and Pagliarini, D.J. (2021). UbiB proteins regulate cellular CoQ distribution in Saccharomyces
819 cerevisiae. Nat Commun *12*, 4769.
820 Khosravi, S., and Harner, M.E. (2020). The MICOS complex, a structural element of mitochondria with
821 versatile functions. Biol Chem.
822 Klecker, T., Bockler, S., and Westermann, B. (2014). Making connections: interorganelle contacts
823 orchestrate mitochondrial behavior. Trends Cell Biol *24*, 537-545.
824 Klecker, T., and Westermann, B. (2021). Pathways shaping the mitochondrial inner membrane. Open
825 Biol *11*, 210238.
826 Knop, M., Siegers, K., Pereira, G., Zachariae, W., Winsor, B., Nasmyth, K., and Schiebel, E. (1999).
827 Epitope tagging of yeast genes using a PCR-based strategy: more tags and improved practical routines.
828 Yeast *15*, 963-972.
829 Korner, C., Barrera, M., Dukanovic, J., Eydt, K., Harner, M., Rabl, R., Vogel, F., Rapaport, D., Neupert,
830 W., and Reichert, A.S. (2012). The C-terminal domain of Fcj1 is required for formation of crista junctions
831 and interacts with the TOB/SAM complex in mitochondria. Mol Biol Cell *23*, 2143-2155.
832 Kornmann, B. (2020). The endoplasmic reticulum-mitochondria encounter structure: coordinating lipid
833 metabolism across membranes. Biol Chem *401*, 811-820.
834 Kornmann, B., Currie, E., Collins, S.R., Schuldiner, M., Nunnari, J., Weissman, J.S., and Walter, P. (2009).
835 An ER-mitochondria tethering complex revealed by a synthetic biology screen. Science *325*, 477-481.

836 Kornmann, B., Osman, C., and Walter, P. (2011). The conserved GTPase Gem1 regulates endoplasmic
837 reticulum-mitochondria connections. Proc Natl Acad Sci U S A *108*, 14151-14156.
838 Lauffer, S., Mabert, K., Czupalla, C., Pursche, T., Hoflack, B., Rodel, G., and Krause-Buchholz, U. (2012).
839 Saccharomyces cerevisiae porin pore forms complexes with mitochondrial outer membrane proteins
840 Om14p and Om45p. J Biol Chem *287*, 17447-17458.
841 Longtine, M.S., McKenzie, A., 3rd, Demarini, D.J., Shah, N.G., Wach, A., Brachat, A., Philippsen, P., and
842 Pringle, J.R. (1998). Additional modules for versatile and economical PCR-based gene deletion and
843 modification in Saccharomyces cerevisiae. Yeast *14*, 953-961.
844 Macinga, D.R., Cook, G.M., Poole, R.K., and Rather, P.N. (1998). Identification and characterization of
845 aarF, a locus required for production of ubiquinone in Providencia stuartii and Escherichia coli and for
846 expression of 2'-N-acetyltransferase in P. stuartii. J Bacteriol *180*, 128-135.
847 Malinverni, J.C., and Silhavy, T.J. (2009). An ABC transport system that maintains lipid asymmetry in
848 the gram-negative outer membrane. Proc Natl Acad Sci U S A *106*, 8009-8014.
849 Miyata, N., Fujii, S., and Kuge, O. (2018). Porin proteins have critical functions in mitochondrial
850 phospholipid metabolism in yeast. J Biol Chem *293*, 17593-17605.
851 Modi, S., Lopez-Domenech, G., Halff, E.F., Covill-Cooke, C., Ivankovic, D., Melandri, D., Arancibia-
852 Carcamo, I.L., Burden, J.J., Lowe, A.R., and Kittler, J.T. (2019). Miro clusters regulate ER-mitochondria
853 contact sites and link cristae organization to the mitochondrial transport machinery. Nat Commun *10*,
854 4399.
855 Mollet, J., Delahodde, A., Serre, V., Chretien, D., Schlemmer, D., Lombes, A., Boddaert, N., Desguerre,
856 I., de Lonlay, P., de Baulny, H.O*., et al.* (2008). CABC1 gene mutations cause ubiquinone deficiency with
857 cerebellar ataxia and seizures. Am J Hum Genet *82*, 623-630.
858 Morgenstern, M., Stiller, S.B., Lubbert, P., Peikert, C.D., Dannenmaier, S., Drepper, F., Weill, U., Hoss,
859 P., Feuerstein, R., Gebert, M*., et al.* (2017). Definition of a High-Confidence Mitochondrial Proteome
860 at Quantitative Scale. Cell Rep *19*, 2836-2852.
861 Murley, A., Sarsam, R.D., Toulmay, A., Yamada, J., Prinz, W.A., and Nunnari, J. (2015). Ltc1 is an ER-
862 localized sterol transporter and a component of ER-mitochondria and ER-vacuole contacts. J Cell Biol
863 *209*, 539-548.
864 Odendall, F., Backes, S., Tatsuta, T., Weill, U., Schuldiner, M., Langer, T., Herrmann, J.M., Rapaport, D.,
865 and Dimmer, K.S. (2019). The mitochondrial intermembrane space-facing proteins Mcp2 and Tgl2 are
866 involved in yeast lipid metabolism. Mol Biol Cell *30*, 2681-2694.
867 Ozbalci, C., Sachsenheimer, T., and Brugger, B. (2013). Quantitative analysis of cellular lipids by nano-
868 electrospray ionization mass spectrometry. Methods Mol Biol *1033*, 3-20.
869 Papagiannidis, D., Bircham, P.W., Luchtenborg, C., Pajonk, O., Ruffini, G., Brugger, B., and Schuck, S.
870 (2021). Ice2 promotes ER membrane biogenesis in yeast by inhibiting the conserved lipin phosphatase
871 complex. EMBO J *40*, e107958.
872 Paumard, P., Vaillier, J., Coulary, B., Schaeffer, J., Soubannier, V., Mueller, D.M., Brethes, D., di Rago,
873 J.P., and Velours, J. (2002). The ATP synthase is involved in generating mitochondrial cristae
874 morphology. Embo J *21*, 221-230.
875 Phillips, M.J., and Voeltz, G.K. (2016). Structure and function of ER membrane contact sites with other
876 organelles. Nat Rev Mol Cell Biol *17*, 69-82.
877 Poon, W.W., Davis, D.E., Ha, H.T., Jonassen, T., Rather, P.N., and Clarke, C.F. (2000). Identification of
878 Escherichia coli ubiB, a gene required for the first monooxygenase step in ubiquinone biosynthesis. J
879 Bacteriol *182*, 5139-5146.
880 Pu, J., Ha, C.W., Zhang, S., Jung, J.P., Huh, W.K., and Liu, P. (2011). Interactomic study on interaction
881 between lipid droplets and mitochondria. Protein Cell *2*, 487-496.
882 Qian, W., Ma, D., Xiao, C., Wang, Z., and Zhang, J. (2012). The genomic landscape and evolutionary
883 resolution of antagonistic pleiotropy in yeast. Cell Rep *2*, 1399-1410.
884 Rabl, R., Soubannier, V., Scholz, R., Vogel, F., Mendl, N., Vasiljev-Neumeyer, A., Korner, C., Jagasia, R.,
885 Keil, T., Baumeister, W*., et al.* (2009). Formation of cristae and crista junctions in mitochondria depends
886 on antagonism between Fcj1 and Su e/g. J Cell Biol *185*, 1047-1063.

887 Reidenbach, A.G., Kemmerer, Z.A., Aydin, D., Jochem, A., McDevitt, M.T., Hutchins, P.D., Stark, J.L.,
888 Stefely, J.A., Reddy, T., Hebert, A.S.*, et al.* (2018). Conserved Lipid and Small-Molecule Modulation of
889 COQ8 Reveals Regulation of the Ancient Kinase-like UbiB Family. Cell Chem Biol *25*, 154-165 e111.
890 Renne, M.F., and Hariri, H. (2021). Lipid Droplet-Organelle Contact Sites as Hubs for Fatty Acid
891 Metabolism, Trafficking, and Metabolic Channeling. Front Cell Dev Biol *9*, 726261.
892 Sakaue, H., Shiota, T., Ishizaka, N., Kawano, S., Tamura, Y., Tan, K.S., Imai, K., Motono, C., Hirokawa, T.,
893 Taki, K.*, et al.* (2019). Porin Associates with Tom22 to Regulate the Mitochondrial Protein Gate
894 Assembly. Mol Cell *73*, 1044-1055 e1048.
895 Schleyer, M., and Neupert, W. (1985). Transport of proteins into mitochondria: translocational
896 intermediates spanning contact sites between outer and inner membranes. Cell *43*, 339-350.
897 Schwaiger, M., Herzog, V., and Neupert, W. (1987). Characterization of translocation contact sites
898 involved in the import of mitochondrial proteins. J Cell Biol *105*, 235-246.
899 Sesaki, H., Dunn, C.D., Iijima, M., Shepard, K.A., Yaffe, M.P., Machamer, C.E., and Jensen, R.E. (2006).
900 Ups1p, a conserved intermembrane space protein, regulates mitochondrial shape and alternative
901 topogenesis of Mgm1p. J Cell Biol *173*, 651-658.
902 Sesaki, H., Southard, S.M., Yaffe, M.P., and Jensen, R.E. (2003). Mgm1p, a dynamin-related GTPase, is
903 essential for fusion of the mitochondrial outer membrane. Mol Biol Cell *14*, 2342-2356.
904 Sikorski, R.S., and Hieter, P. (1989). A system of shuttle vectors and yeast host strains designed for
905 efficient manipulation of DNA in Saccharomyces cerevisiae. Genetics *122*, 19-27.
906 Stefely, J.A., Reidenbach, A.G., Ulbrich, A., Oruganty, K., Floyd, B.J., Jochem, A., Saunders, J.M.,
907 Johnson, I.E., Minogue, C.E., Wrobel, R.L.*, et al.* (2015). Mitochondrial ADCK3 employs an atypical
908 protein kinase-like fold to enable coenzyme Q biosynthesis. Mol Cell *57*, 83-94.
909 Stenger, M., Le, D.T., Klecker, T., and Westermann, B. (2020). Systematic analysis of nuclear gene
910 function in respiratory growth and expression of the mitochondrial genome in S. cerevisiae. Microb
911 Cell *7*, 234-249.
912 Strauss, M., Hofhaus, G., Schroder, R.R., and Kuhlbrandt, W. (2008). Dimer ribbons of ATP synthase
913 shape the inner mitochondrial membrane. EMBO J *27*, 1154-1160.
914 Subramanian, K., Jochem, A., Le Vasseur, M., Lewis, S., Paulson, B.R., Reddy, T.R., Russell, J.D., Coon,
915 J.J., Pagliarini, D.J., and Nunnari, J. (2019). Coenzyme Q biosynthetic proteins assemble in a substrate-
916 dependent manner into domains at ER-mitochondria contacts. J Cell Biol *218*, 1353-1369.
917 Tamura, Y., Endo, T., Iijima, M., and Sesaki, H. (2009). Ups1p and Ups2p antagonistically regulate
918 cardiolipin metabolism in mitochondria. J Cell Biol *185*, 1029-1045.
919 Tamura, Y., Kawano, S., and Endo, T. (2019). Organelle contact zones as sites for lipid transfer. J
920 Biochem *165*, 115-123.
921 Tamura, Y., Onguka, O., Hobbs, A.E., Jensen, R.E., Iijima, M., Claypool, S.M., and Sesaki, H. (2012). Role
922 for two conserved intermembrane space proteins, Ups1p and Ups2p, [corrected] in intra-
923 mitochondrial phospholipid trafficking. J Biol Chem *287*, 15205-15218.
924 Tan, T., Ozbalci, C., Brugger, B., Rapaport, D., and Dimmer, K.S. (2013). Mcp1 and Mcp2, two novel
925 proteins involved in mitochondrial lipid homeostasis. J Cell Sci *126*, 3563-3574.
926 Thong, S., Ercan, B., Torta, F., Fong, Z.Y., Wong, H.Y., Wenk, M.R., and Chng, S.S. (2016). Defining key
927 roles for auxiliary proteins in an ABC transporter that maintains bacterial outer membrane lipid
928 asymmetry. Elife *5*.
929 Tirrell, P.S., Nguyen, K.N., Luby-Phelps, K., and Friedman, J.R. (2020). MICOS subcomplexes assemble
930 independently on the mitochondrial inner membrane in proximity to ER contact sites. J Cell Biol *219*.
931 Unger, A.K., Geimer, S., Harner, M., Neupert, W., and Westermann, B. (2017). Analysis of Yeast
932 Mitochondria by Electron Microscopy. Methods Mol Biol *1567*, 293-314.
933 van der Laan, M., Bohnert, M., Wiedemann, N., and Pfanner, N. (2012). Role of MINOS in mitochondrial
934 membrane architecture and biogenesis. Trends Cell Biol *22*, 185-192.
935 von der Malsburg, K., Muller, J.M., Bohnert, M., Oeljeklaus, S., Kwiatkowska, P., Becker, T., Loniewska-
936 Lwowska, A., Wiese, S., Rao, S., Milenkovic, D.*, et al.* (2011). Dual role of mitofilin in mitochondrial
937 membrane organization and protein biogenesis. Dev Cell *21*, 694-707.

938 Vyssokikh, M.Y., and Brdiczka, D. (2003). The function of complexes between the outer mitochondrial
939 membrane pore (VDAC) and the adenine nucleotide translocase in regulation of energy metabolism
940 and apoptosis. Acta Biochim Pol *50*, 389-404.
941 Wenz, L.S., Opalinski, L., Schuler, M.H., Ellenrieder, L., Ieva, R., Bottinger, L., Qiu, J., van der Laan, M.,
942 Wiedemann, N., Guiard, B*., et al.* (2014). The presequence pathway is involved in protein sorting to
943 the mitochondrial outer membrane. EMBO Rep *15*, 678-685.
944 Westermann, B., and Neupert, W. (2000). Mitochondria-targeted green fluorescent proteins:
945 convenient tools for the study of organelle biogenesis in Saccharomyces cerevisiae. Yeast *16*, 1421-
946 1427.
947 Wittig, I., Braun, H.P., and Schagger, H. (2006). Blue native PAGE. Nat Protoc *1*, 418-428.
948 Wong, E.D., Wagner, J.A., Scott, S.V., Okreglak, V., Holewinske, T.J., Cassidy-Stone, A., and Nunnari, J.
949 (2003). The intramitochondrial dynamin-related GTPase, Mgm1p, is a component of a protein complex
950 that mediates mitochondrial fusion. J Cell Biol *160*, 303-311.
951 Xie, J., Marusich, M.F., Souda, P., Whitelegge, J., and Capaldi, R.A. (2007). The mitochondrial inner
952 membrane protein mitofilin exists as a complex with SAM50, metaxins 1 and 2, coiled-coil-helix coiled-
953 coil-helix domain-containing protein 3 and 6 and DnaJC11. FEBS Lett *581*, 3545-3549.
954 Xie, L.X., Ozeir, M., Tang, J.Y., Chen, J.Y., Jaquinod, S.K., Fontecave, M., Clarke, C.F., and Pierrel, F.
955 (2012). Overexpression of the Coq8 kinase in Saccharomyces cerevisiae coq null mutants allows for
956 accumulation of diagnostic intermediates of the coenzyme Q6 biosynthetic pathway. J Biol Chem *287*,
957 23571-23581.
958 Xu, L., Xie, Q., Qi, L., Wang, C., Xu, N., Liu, W., Yu, Y., Li, S., and Xu, Y. (2018). Bcl-2 overexpression
959 reduces cisplatin cytotoxicity by decreasing ER-mitochondrial Ca2+ signaling in SKOV3 cells. Oncol Rep
960 *39*, 985-992.
961 Zerbes, R.M., Bohnert, M., Stroud, D.A., von der Malsburg, K., Kram, A., Oeljeklaus, S., Warscheid, B.,
962 Becker, T., Wiedemann, N., Veenhuis, M*., et al.* (2012). Role of MINOS in mitochondrial membrane
963 architecture: cristae morphology and outer membrane interactions differentially depend on mitofilin
964 domains. J Mol Biol *422*, 183-191.
965 Zick, M., Duvezin-Caubet, S., Schafer, A., Vogel, F., Neupert, W., and Reichert, A.S. (2009). Distinct roles
966 of the two isoforms of the dynamin-like GTPase Mgm1 in mitochondrial fusion. FEBS Lett *583*, 2237-
967 2243.

968

969